Climatic reconstruction for the Younger Dryas/Early Holocene transition and the Little Ice Age based on paleo-extents of Argentière glacier (French Alps)

Marie Protin, Irene Schimmelpfennig, Jean-louis Mugnier, Ludovic Ravanel, Melaine Le Roy, Philip Deline, Vincent Favier, Jean-François Buoncristiani, Team Aster, Didier Bourlès, et al.

Climatic reconstruction for the Younger Dryas/Early Holocene transition and the Little Ice Age based on paleo-extents of Argentière glacier (French Alps)

Marie Protin[a], Irene Schimmelpfennig[a], Jean-Louis Mugnier[b], Ludovic Ravanel[c], Melaine Le Roy[c], Philip Deline[c], Vincent Favier[d], Jean-François Buoncristiani[e], ASTER Team[a]

[a] Aix-Marseille Univ, CNRS, IRD, INRA, Coll France, CEREGE, Aix-en-Provence, 13545, France

[b] Université Grenoble Alpes, Université Savoie Mont Blanc, CNRS, ISTerre, Chambéry, 73000, France

[c] Université Grenoble Alpes, Université Savoie Mont Blanc, CNRS, EDYTEM, Chambéry, 73000, France

[d] Université Grenoble Alpes, CNRS, IRD, Grenoble INP, IGE, Grenoble, France

[e] Biogéosciences, UMR 6282 CNRS, Université Bourgogne Franche-Comté, 6 Boulevard Gabriel, Dijon, 21000, France

Consortium: ASTER Team (Georges Aumaître, Didier Bourlès, Karim Keddadouche)

Correspondence to: Marie Protin (protin@cerege.fr)

Abstract

Investigation of Holocene extents of mountain glaciers along with the related naturally-driven climate conditions helps improve our understanding of glacier sensitivity to ongoing climate

change. Here, we present the first Holocene glacial chronology in the Mont-Blanc massif (Argentière glacier) in the French Alps, based on 25 *in situ*-produced cosmogenic ^{10}Be dates of moraines and glacial bedrocks. The obtained ages from mapped sequences of moraines at three locations reveal that the glacier was retreating from its Lateglacial extent and oscillating several times between ~11.7 ka and ~10.4 ka, i.e. during the Younger Dryas/Early Holocene (YD/EH) transition, before substantially retreating at ~10.4 ka. Climate conditions corresponding to the past extents of Argentière glacier during the YD/EH transition (~ 11 ka) and the Little Ice Age (LIA) were modelled with two different approaches: by determining summer temperature differences from reconstructed ELA-rises and by using a Positive Degree Day (PDD) mass-balance model coupled with a dynamic ice flow model. The ELA-rise reconstructions yield a possible range of summer temperatures for the YD/EH transition that were cooler by between 3.0 and 4.8°C compared to the year 2008, depending on the choice of the ELA sensitivity to summer temperature. The results from the PDD model indicate temperatures cooler by ~3.6 to 5.5°C during the YD/EH transition than during the 1979-2002 period. For the LIA, our findings highlight that the role of local precipitation changes, superimposed on the dominant temperature signal, is important in the detailed evolution of the glacier. Overall, this study highlights the challenge that remains in accurately inferring paleoclimate conditions from past glacier extents.

Keywords

Holocene; Glaciation; Western Europe; Cosmogenic nuclides; Glacier fluctuations; French Alps; Moraine dating; Paleoclimate reconstruction; PDD modeling

1. Introduction

Investigating natural climate changes during the Holocene is relevant for assessing the impact of the current climate changes, because Holocene climate variations were similar in amplitude to the ones that are historically observed and predicted for the next few decades (e.g. Marcott et al., 2013). Mountain glaciers are known to be sensitive climate change indicators (Oerlemans, 2005), as their dynamics in the mid-latitudes, e.g. in the European Alps, depend both on summer temperature and winter precipitation variations. They thus represent a highly useful proxy for Holocene climate reconstructions. The ongoing trend of global glacier retreat, which started after the end of the Little Ice Age (LIA), in the middle of the 19th century, is well recorded with instrumental measurements (Leclercq et al., 2014). Evidence of pre-instrumental glacier fluctuations are recorded by glacial landforms, which provide the opportunity to reconstruct past glacier chronologies and examine glacier-climate interactions over a longer period. In particular, moraine deposits give valuable information about past glacier extents and dating them using *in situ* cosmogenic nuclides allows us to put glacier variations into a spatio-chronological framework. Over the past few years, a growing number of studies in the Alps have reported advanced glacier positions during the Late Glacial and Holocene relying on *in situ*-produced cosmogenic beryllium-10 (^{10}Be) moraine dating (e.g. Moran et al., 2016; Schimmelpfennig et al., 2014; Schindelwig et al., 2012). In several of these studies, the corresponding equilibrium line altitudes (ELA) were estimated (e.g. Baroni et al., 2017; Hofmann et al., 2019; Le Roy et al., 2017). As the ELA directly depends on the climate, in particular on atmospheric temperature and precipitation, reconstruction of past ELAs provides the opportunity to estimate paleoclimate conditions. Atmospheric temperature variations can be inferred using the adiabatic lapse rate or an ELA sensibility to atmospheric temperature, as has previously been done in the Alps by Hofmann et al. (2019), Le Roy et al. (2017) and Moran et al. (2016). However, this approach assumes that the impact of precipitation on the glacier behavior is negligible or that the precipitation amount did not

change through time, potentially leading to a bias in the deduced temperature variations. In the Alps, only few studies have attempted so far to infer precipitation changes from past glacier extents (e.g. Keeler, 2015; Kerschner and Ivy-Ochs, 2007), as disentangling the detailed contributions of both precipitation and temperature changes to glacier fluctuations is still difficult (Solomina et al., 2016).

In this study, we explore the frontal and lateral moraines, as well as roches moutonnées located beyond the limits of the LIA extent of Argentière glacier with the objective to present the first alpine Holocene glacier chronology based on ^{10}Be dating in the Mont-Blanc massif. Potential climatic conditions corresponding to past extents of Argentière glacier are determined using two different approaches, including a PDD mass-balance model, which allows considering both precipitation and temperature variations.

2. Study site, geomorphologic setting and previous work on the past fluctuations of Argentière glacier

Argentière glacier (45°55'N, 6°57'E), located on the north-western side of the Mont Blanc massif, is the second largest glacier in the French Alps (Figure 1). In 2008, it covered a surface of ~14 km^2 with a length of almost 10 km and an altitude range spanning 3530 m to 1550 m a.s.l. (Six and Vincent, 2014; Vincent et al., 2009). Since 2009, the tongue (7 % of the glacier area) is disconnected from the main glacier body and remains fed by an icefall located at ~2200 m a.s.l. This tongue is covered by debris since at least the middle of the 20th century (aerial photography from IGN, https://remonterletemps.ign.fr), while it was uncovered in the middle of the 19th century according to pictorial documents from the LIA (Fontaine, 2015). The ELA has been measured at ~2890 m a.s.l. between 1995 and 2011 (Six and Vincent, 2014). The mean annual temperature and precipitation were 6.5°C and 1238 mm in Chamonix - Le Bouchet, the nearest weather station located at 1042 m a.s.l. for the time period 1961-

1990 (Météo France) and are estimated at 1.8°C and 1783 mm at ~2000 m a.s.l. next to Argentière glacier for the time period 1979-2002 (Joly et al., 2018 and personal communication of D. Joly). Snow accumulation on the glacier at 3000 m a.s.l. is known to be 3 times larger than valley precipitation due to the orographic effect on precipitation, impact of the wind and of avalanches, as the glacier is surrounded by steep slopes (Six and Vincent, 2014). Climatic data began to be collected in the Alpine region in the year 1760 (temperature measurements) and in the year 1800 (precipitation) and are compiled in the HISTALP project (http://www.zamg.ac.at/histalp/; Auer et al., 2007).

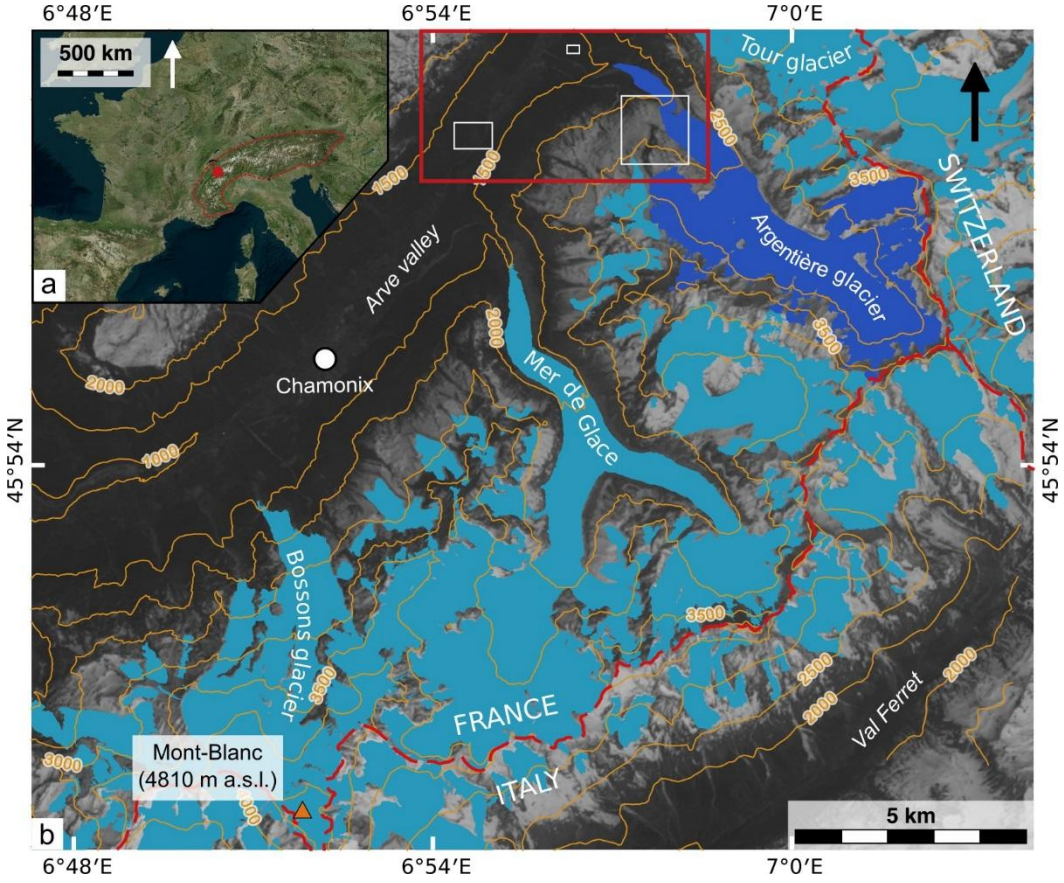

Figure 1 : General overview of the study area. (a) Location of the Mont Blanc massif (red dot) in the Alps (red dotted line). (b) Landsat 8 image of the Mont Blanc massif from April 2005, with the 2008 extent of glaciers in blue. French glaciers: Gardent et al. (2014); Swiss glaciers: Fischer et al. (2014); Italian glaciers: Smiraglia et al. (2015). Argentière glacier is highlighted in dark blue. Red dotted lines represent countries borders. Red square represents

the location of Figure 2 and white squares represent the sampling locations, shown in Figure 7.

The Argentière glacier catchment is mainly formed by granite from the late Hercynian along with Variscan metamorphic rocks (Bussy et al., 2000). Numerous preserved moraine ridges and moraine remnants are visible in the catchment, close to the glacier, and downstream in the Arve valley providing evidence of the past fluctuations of Argentière glacier (Figure 2). While it's behavior since the LIA is well-known (Bless, 1984; Payot, 1884; Vincent et al., 2009), few chronological data constrain its Holocene fluctuations prior to the 17th century (Bless, 1984; Le Roy, 2012). During the Last Glacial Maximum (LGM), the valleys around the Mont Blanc massif were glacierized, and the glacier surface reached an altitude of 2400 m a.s.l. at the location of Argentière glacier, as reconstructed from the trimline positions in the region of the Mont Blanc massif (Figure 2, Coutterand and Buoncristiani, 2006). During the Late-Glacial, glaciers located on the western flank of the Mont-Blanc massif were still connected as one glacier named Arve glacier, extending in the Arve valley over a distance of 30 km, where numerous and mostly lateral moraine relicts attest to multiple glacier fluctuations during that period (Coutterand and Nicoud, 2005). At one point during the retreat from the large Late-Glacial glacier extents, Argentière glacier disconnected from its neighbors Mer de Glace and Tour Glacier, which is revealed by two latero-frontal moraines sets near *La Joux* et near *Le Planet* in the Arve valley (Figure 2). Due to the lack of direct dating methods, 20th century studies on past glacier fluctuations were often based on the comparison of ELA depressions, geomorphic moraine characteristics, pollen analyses or limiting radiocarbon dates to correlate moraines within regionally defined relative glacier chronologies like the "stadials" of the classical Swiss alpine terminology (e.g. Maisch, 1981). Such relative dating was applied to the extent of Le Tour and Argentière glaciers and several interpretations suggest that these moraines were deposited during the Late-Glacial or Early Holocene (Jaillet

and Ballandras, 1999; Lucéna and Ballandras, 1999; Bless, 1984), although there is no indication for an univocal correlation to the classical Swiss alpine nomenclature. Further evidence of Argentière glacier variations during the Holocene are provided by Bless (1984) and Le Roy (2012). Radiocarbon dating of subfossil organic material found in stratigraphic position in the right-lateral composite moraine (yellow dot on Figure 2) gave evidence of five glacier advances between ~4 ka and 1.2 ka, *i.e.* during the so-called Neoglacial, a period when the climatic conditions became more suitable for glacial advances (Bless, 1984). In the same moraine profile, dating of detrital wood embedded-in-till 30 years later, indicates an advance during the 9th century, similar in elevation to the LIA maxima (Le Roy, 2012). Finally, Argentière glacier reached its LIA frontal maximum extent during the 17th century, according to several written reports about the destruction or menace of villages by the advancing glacier (Bless, 1984).

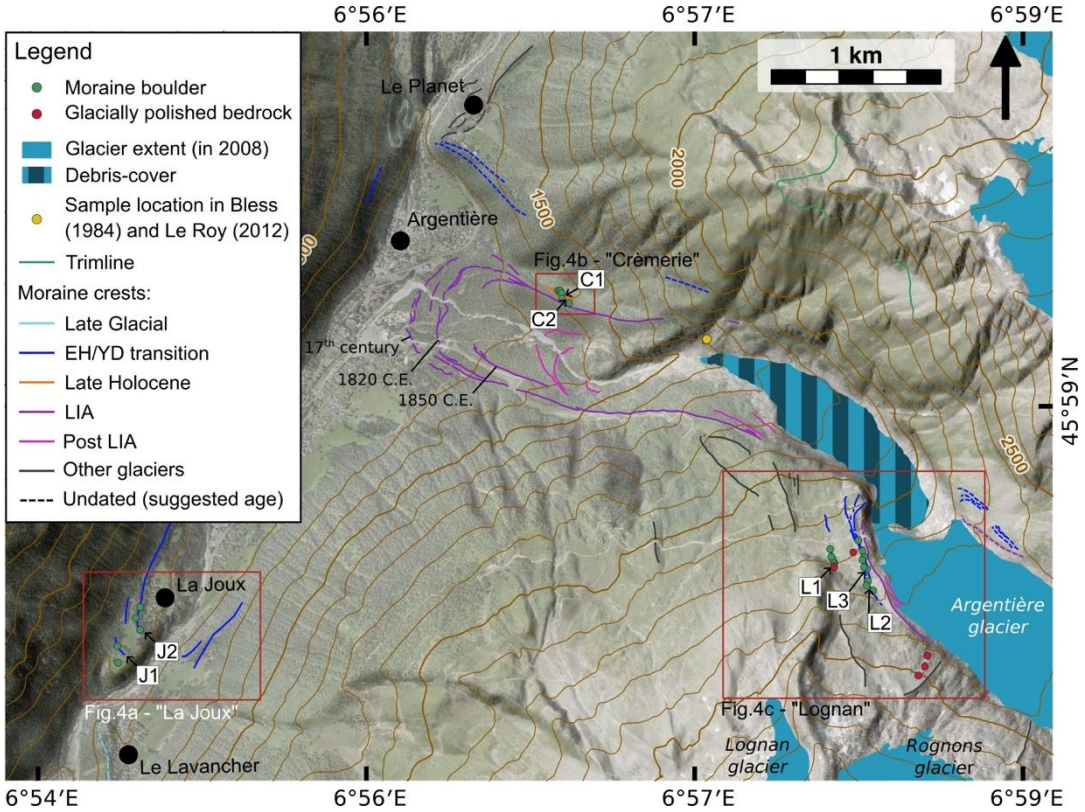

Figure 2 : Geomorphic map of the study area with individual sample locations on the 5 m IGN DEM RGE ALTI. The 2008 extent of Argentière and nearby glaciers are represented in

blue (Gardent et al., 2014). Geomorphologic features were mapped based on Bless (1984) and Le Roy (2012), DEM interpretation and field observations. Dashed lines represent undated moraines, their ages are presumed from their position relative to moraines of known ages; grey lines are moraines attributed to nearby glaciers.

3. Methodology

3.1. Moraine mapping

The geomorphologic map presented in Figure 2 was produced using Geographic Information System (GIS). It is based on field observations along with interpretation of recent aerial images (from the IGN, 50 cm resolution) and LIDAR digital elevation models (DEM), with resolution of 1 m (Arve valley) and 2 m (Argentière catchment). The map in Figure 2 also includes moraines that were mapped in earlier studies (Le Roy, 2012; Bless, 1984).

3.2. Sampling and cosmogenic ^{10}Be ages

All samples were obtained using a cordless angle grinder, chisel and hammer (Figure 3). Boulder samples were collected from the top of boulders embedded in the crests or on the slopes of selected moraines and bedrock samples were preferentially taken from sloping surfaces to minimize the risk of cover by vegetation, sediment or snow (Figure 3). We only sampled surfaces with minimal signs of erosion, exhibiting glacial striation when possible, and moraine boulders that were big enough (>1 m) to avoid the risk of exhumation. In total, 20 moraine boulders and 5 bedrock samples were collected. Topographic shielding was determined in the field using a clinometer.

The chemical procedure for ^{10}Be extraction from the rock was conducted at CEREGE (Aix-en-Provence, France). Samples were crushed and sieved to the 250-500 µm fraction. Quartz was isolated from other grains first by magnetic separation, then either by repeated leaching

in a H_2SiF_6/HCl mixture or by froth flotation, and finally by at least three sequential leaching steps in concentrated HF to remove remaining feldspar grains and atmospheric ^{10}Be. About 0.1 g of a 3025 ± 9 ppm in-house ^{9}Be carrier solution (Merchel et al., 2008) was added to the purified quartz before its complete dissolution in concentrated HF. Beryllium was extracted and purified by separation on anion and cation columns and by successive alkaline precipitations of $Be(OH)_2$, and the samples were then oxidized for one hour at 700°C. The final BeO oxides were mixed with Nb powder and loaded into nickel cathodes for AMS measurements. The $^{10}Be/^{9}Be$ ratios of all samples were measured at the French national AMS facility ASTER (Arnold et al., 2010) and calibrated against in-house standard STD-11 with an assigned $^{10}Be/^{9}Be$ ratio of $(1.191 \pm 0.013) \times 10^{-11}$ (Braucher et al., 2015) using the ^{10}Be half-life of $(1.387 \pm 0.0012) \times 10^{6}$ years (Chmeleff et al., 2010; Korschinek et al., 2010). Analytical uncertainties due to AMS measurement include ASTER counting statistics and stability (~0.5 %; Arnold et al. (2010)) and blank correction. Correction for the chemical blanks, whose $^{10}Be/^{9}Be$ ratios range between $(3.21 \pm 0.50) \times 10^{-15}$ and $(4.87 \pm 0.63) \times 10^{-15}$, were performed by subtracting their numbers of atoms ^{10}Be from those of the samples calculated from the $^{10}Be/^{9}Be$ ratios (Table 1).

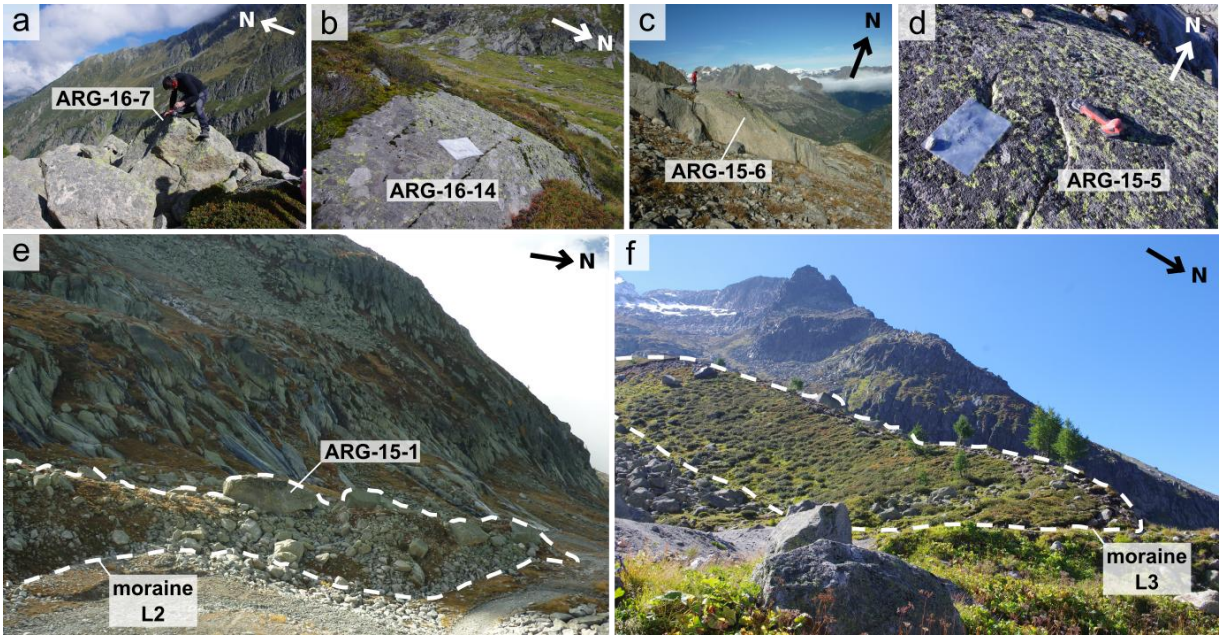

Figure 3 : Photographs of sample sites at Argentière glacier. Example of (a) moraine boulder (ARG-16-7), (b) inter-morainic bedrock surface and (c) roche moutonnée (ARG-15-6) along with (d) roche moutonnée surface (ARG-15-5) sample from Lognan area. View of dated moraines (e) L2 and (f) L3 (framed by the dashed line) located in the left-lateral Lognan area.

Surface exposure ages were calculated with the CREp online calculator (Martin et al., 2017) applying the Lal-Stone time corrected scaling scheme, the ERA40 Atmosphere model and the Atmospheric ^{10}Be-based VDM for geomagnetic database (see Martin et al. (2017) and references therein). The "Alpine" ^{10}Be production rate of 4.11 ± 0.10 atoms ^{10}Be/g established by Claude et al. (2014) was retained here as it is the only available regional production rate. In addition, it yields results very similar to the NENA production rate (Balco et al., 2009), which has often been used in previous studies in the Alps and has a value of 4.10 ± 0.17 atoms ^{10}Be/g when recalculated in CREp with the above parameters. We note that the "Arctic" production rate (Young et al., 2013; 4.12 ± 0.25 atoms ^{10}Be/g according to CREp), also used for several alpine studies, would lead to ages younger by ~ 0.25 %. Calculated exposure ages are presented in Table 1. We did not correct the ages for snow cover effects or surface erosion, as these effects were minimized by sampling boulders least likely to have

been snow covered and with minimal signs of erosion. Applying a high snow cover correction corresponding to 50 cm of snow for 6 months, as used in Chenet et al. (2016), would lead to ages older by ≤ 8 % and assuming an erosion rate of 1 mm.kyr^{-1} (André, 2002) would lead to ages older by only 1%. Nonetheless, the presented ages should be considered minimum exposure ages.

3.3. Glacier reconstruction and paleoclimatic modelling

Two approaches were used to infer paleoclimatic conditions from the extents of Argentière glacier. Both approaches are based on the simplified assumption that the glacier is in equilibrium with the climate conditions during the respective present-day reference periods detailed below.

3.3.1. GIS-based ELA reconstruction and paleo-temperature determination

In the first approach, 3D glacier surface reconstructions were generated for different glacier extents in the past using the ArcGIS toolbox GlaRe (Pellitero et al., 2016) based on the mapping of the moraines presented in Figure 2. The topography of the bedrock beneath of Argentière glacier used for the reconstruction was determined by subtracting the ice thickness (Rabatel et al., 2018) from the 25 m IGN DEM BD Alti. ELA calculations were then done using the ArcGIS toolbox developed by Pellitero et al. (2015) according to the Area-Altitude Balance Ratio (AABR) with a balance ratio of 1.59 and the Accumulation Area Ratio (AAR) method with a ratio of 0.67, both values representative for the Alps (Pellitero et al., 2015; Rea, 2009). While the AAR methods is simply based on the ratio between the surface of the accumulation area and the surface of the entire glacier, the AABR method take into account the hypsometry of the glacier (Osmaston, 2005) and the mass balance gradient (Benn and Lehmkuhl, 2000) and is therefore considered more reliable to approximate ELAs (Lukas, 2007; Pellitero et al., 2015). However, the AAR method has most often been used in the Alps (e.g. Hofmann et al., 2019; Le Roy et al., 2017; Moran et al., 2016). Thus, for the

paleoclimatic discussion we prefer the results inferred from the ELAs calculated with the AABR method and the results from the AAR method are only used for the sake of comparison with other Alpine sites. We adjusted the shear stress value along the flowlines in the ArcGIS toolbox GlaRe (Pellitero et al., 2016) by comparing the ELA calculated for the 2008 extent of Argentière glacier to the mean ELA measured in the field between 1995 and 2011 (~2890 m, Six and Vincent, 2014). The best estimate are found for a shear stress value of 150 kPa and an automatic shape factor. The calculated ELAs for the 2008 extent are 2866 m using the AABR method and 2801 m using the AAR method. These two values are close, yet inferior, to the measured ELA. It has to be noted that in 2008 the glacier was not in steady-state, therefore the measured ELA does not reflect an equilibrium position unlike the calculated values, which hinders us from accurately fitting both and might explain the difference between them.

The difference of the resulting paleo-ELAs between two periods allows for determination of the associated variation in atmospheric temperature (T) by using a constant ELA sensitivity to atmospheric temperature (S) and assuming the same precipitation as today, following the equation $\Delta T = \Delta ELA/S$. The ELA sensitivity to summer temperature is nonetheless difficult to estimate and two values are used in this paper: 115 $m°C^{-1}$, which is relevant for French Alpine glaciers (Rabatel et al., 2013); and 72 $m°C^{-1}$, which was empirically quantified for Argentière glacier by Six and Vincent (2014) and takes into account the local effects of temperature and all meteorological parameters that influenced the snow and ice ablation.

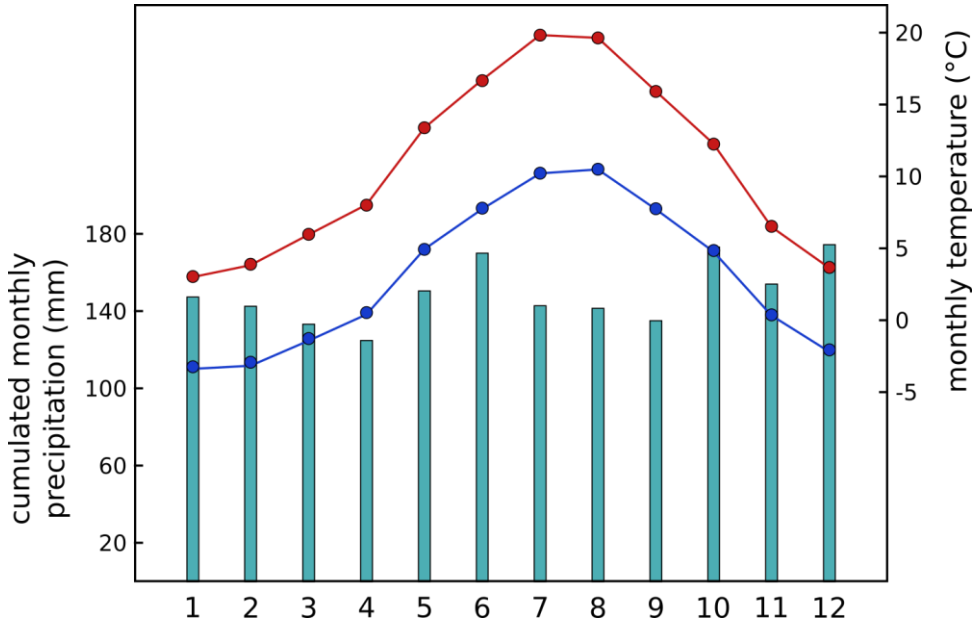

Figure 4 : Climatic data of Argentière glacier between 1979 and 2002 at ~2000 m a.s.l.. Blue bars represent the cumulated monthly precipitation, the blue and red curves represent respectively the minimum and maximum monthly temperatures. 1 to 12 represents the months January to December.

3.3.2 PDD modelling

In the second approach, combinations of precipitation and temperature variations and ELAs for different glacier extents were determined by using a PDD mass-balance model coupled with a dynamic ice flow model, described in Blard et al. (2007). This model has previously been used for glaciers in the central pacific by Blard et al. (2007), in the Andes by Jomelli et al. (2011) and in Greenland by Biette et al. (2018). The topography of the watershed of Argentière glacier used for the modeling is the same used for the GIS-based reconstructions (see section 3.3.1.). The model was calibrated using the mass-balance data from 1979 to 2002 (considered here as the present-day reference period) collected at Argentière glacier by the GlacioClim Network (https://glacioclim.osug.fr) from extensive field measurements on 10 markers distributed along the glacier (5 in the ablation area and 5 in the accumulation area) and local monthly values of temperature and precipitation for the same period (personal

communication of D. Joly), inferred at 2000 m a.s.l. in the Argentière catchment from a downscaling method based on a geomatic spatial model (Joly et al., 2018). Figure 4 depicts the monthly values of temperature and precipitation of Argentière glacier averaged from 1979 to 2002 as used in the model. This interval is nearly twice as long as the 10-14 years response time of the glacier front position to a mass balance change (Vincent et al., 2009) and is long enough to fade out the inter-annual variability. In addition, the glacier length at the beginning of this period is very similar to that at the end, as it includes an advance of the glacier followed by an equal retreat (Figure 5). This consolidates the assumption that the glacier was roughly in equilibrium with the mean climatic condition during this period. This period is put into a broader context and compared to the variations of Argentière glacier since 1800 in Figure 5. The atmospheric lapse rate of temperature and precipitation are fixed at 0.65°C/m and 80mm/100m/year, respectively. This precipitation lapse rate matches best the field data taking into the range of the precipitation lapse rate between precipitation in the valley and at high altitude in the MMB of 52mm/100m/years (Corbel, 1963) as well as the variable ratio between valley precipitation and winter accumulation on Argentière glacier (Six and Vincent, 2014) equivalent to a lapse rate of ~95mm/100m/years.

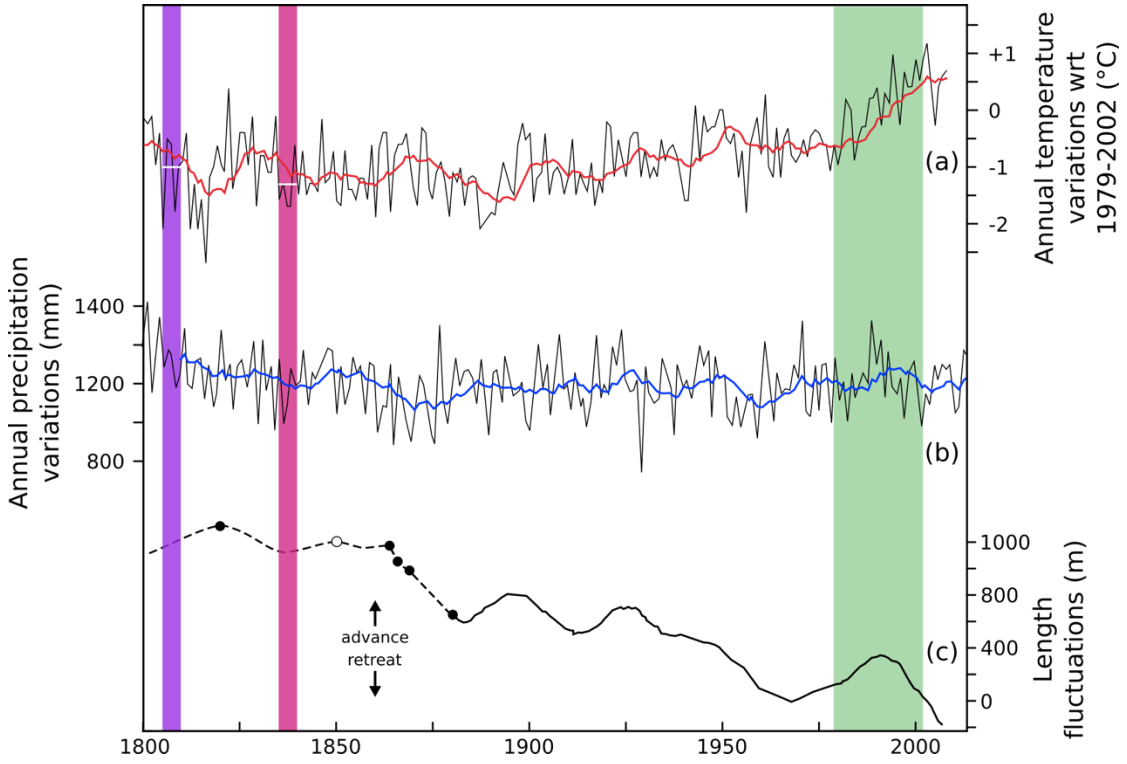

288

289 *Figure 5 : (a) Annual temperature anomalies (reference period 1979-2002); (b) annual*
290 *precipitation in the west part of the Alps from the HISTALP time series (Auer et al., 2007)*
291 *and (c) front variation of the Argentière glacier - the origin of the axis is arbitrary (1818-*
292 *1880: Payot, 1884 in Fontaine, 2015; 1850: Bless (1984); 1880-2000: Francou and Vincent,*
293 *2007; > 2000: Vincent et al., 2009. Red and blue curves represent 10-years running means.*
294 *Period of reference of the climatic data of Argentière glacier (1979-2002) used as input in the*
295 *PDD model is highlighted in green. Periods considered for extracting the temperature values*
296 *for the 1820 and 1850 glacier extents, accounting for the glacier's response time, are*
297 *highlighted in purple and pink, respectively. The extracted mean temperatures are depicted by*
298 *white horizontal lines.*

299 Figure 6 shows the correlation between observed and calculated mass balance of Argentière
300 glacier. This best fit (R^2 = 0.97) was obtained using the least mean square optimization on the
301 determination of the melting factor (MF) used in the PDD model, whose values are MF_{snow} =
302 2.3 mm w.e. $°C^{-1}$ d^{-1} and MF_{ice} = 5.1 mm w.e. $°C^{-1}$ d^{-1}. These values are close to the ones

303 defined in Réveillet et al. (2017) for Argentière glacier: MF_{snow} = 3.5 mm w.e. $°C^{-1}$ d^{-1} and
304 MF_{ice} = 5.5 mm w.e. $°C^{-1}$ d^{-1}. Using these parameters and the climatic inputs presented in
305 Figure 4, the calculated ELA is 2940 m a.s.l., whereas Argentière glacier ELA measurements
306 using satellite images during the years 1984 to 2002 ranged between 2623 and 2861 m a.s.l.
307 (Rabatel et al., 2013). Furthermore, the length of the modeled glacier is between 600 and 300
308 m shorter than that of Argentière glacier between 1990 and 2001. As the lower part of the
309 Argentière glacier is covered by debris from before the middle of the 20^{th} century, and termini
310 of debris-covered glaciers, like the Miage glacier in the Mont Blanc massif (Smiraglia et al.,
311 2010), are often less responsive to climatic variability than non-covered glaciers (Scherler et
312 al., 2011), this might be the reason why the model predicts a shorter length. Nonetheless, due
313 to the excellent agreement between calculated and measured mass balance (Figure 6), we
314 consider that the above calibration of the model is suited for modeling the past extents of the
315 glacier. For each investigated extent, the model considers all potential combinations of
316 precipitation and temperature conditions that lead to a match of the front of the modeled
317 paleo-glacier with the position of the corresponding frontal moraine mapped in the field.
318 ELAs correspond to the altitudes where the glacier mass balance is zero. For each glacier
319 extent, ELAs vary over a range of more than 100 m, due to the large range of assumed
320 precipitation conditions (between 0 and 2 times that of the reference period).

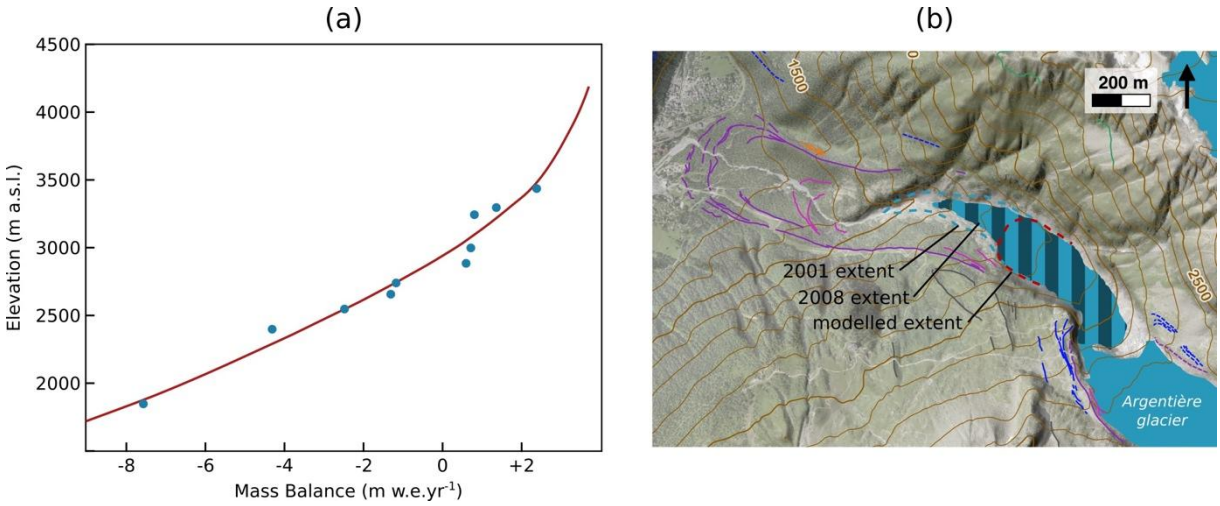

Figure 6: (a) Comparison between observed mass balance (1979-2002; Glacioclim Network) on the Argentière glacier (blue dotes) and mass balance calculated by the PDD model (red curve). (b) Comparison between the modelled glacier extent for the reference period of 1979-2002 (red dotted line), the 2001 extent (blue dotted line; Le Roy, 2012) and the 2008 extent (blue area; Gardent et al., 2014).

4. Results

4.1. Description of the geomorphological evidence

Figure 2 presents a moraine map of the Argentière catchment. The frontal moraines located around 1.5-2 km downstream of the present glacier front (purple moraines in Figure 2) have been assigned by Bless (1984) to four LIA advances between the 17th century and 1850 based on analysis of historical written documents and paintings combined with lichenometry dating. On both lateral sides, the LIA advances are represented by massive composite moraines of up to 80 m height and ≥ 1 km length. Multiple ridges are visible between the ~1850 frontal moraine and the current front, representing the generally gradual retreat of the glacier since the end of the LIA (pink moraines in Figure 2). Immediately to the north, slightly outboard of the right-lateral LIA composite moraine, four short ridges of so far unknown age are preserved (orange moraines in Figure 2). This area, hereafter called "*Crèmerie*", is covered by

a dense conifer forest, but the morphology of the ridges is noticeable on the DEM and attested by a few disseminated moraine boulders.

Further upstream near the present-day Argentière glacier icefall, multiple ridges of lateral moraines are preserved. On the left-lateral side, in the area called "*Lognan*", the most prominent moraine, ~15 m-high and 700 m-long is attributed to the LIA (Figure 2). Only a few tens of meters outboard, two dissected main ridges and several subridges lie tight together (among them L2 and L3 in Figure 2), and another dissected ridge is preserved about 150-200 m further outboard (L1 in Figure 2). According to their positions, these ridges are pre-LIA moraine relicts but were undated until now. They display a smoother morphology than the massive LIA moraine, but are located around the same altitude, and exhibit several boulders suitable for sampling. At their upstream (southern) ends, these moraines abut against a steep and up to a 150 m-high bedrock outcrop, which testifies to past glacial cover owing to numerous roches moutonnées (Figure 3). This roche moutonnée area lies between the current terminus of Rognons glacier and the left-lateral bank of Argentière glacier and is framed by two moraines deposited by Rognons glacier during its retreat. A similar moraine sequence pattern is observed on the north-eastern bank of the glacier. Moraines located further to the west of the pre-LIA deposits in the Lognan area (grey moraines on Figure 2) are not considered as moraines built by Argentière glacier. They were most likely deposited by the Lognan glacier, a smaller nearby glacier. This is suggested by their composition of gneiss boulders, transported from the Lognan glacier catchment, whereas the boulders embedded in the sampled moraines are granitic according to the main lithology of the Argentière glacier catchment.

Downstream in the Arve valley near *La Joux*, relicts of a latero-frontal moraine set are preserved (dark blue moraines in Figure 2). These moraines, smooth and covered by conifer trees, were studied and mapped in detail by Bless (1984) and Lucéna and Ballandras (1999)

365 and named “La Chauffria II” and “La Joux” (Lucéna and Ballandras, 1999), corresponding to
366 J1 and J2 moraines respectively in Figure 2. Furthermore, remnant of at least one other
367 moraine is located between J1 and J2. Some boulders are embedded in these moraines. A set
368 of lateral ridges are observed along the right-lateral valley flanks on the NW side of the
369 Argentière glacier catchment, especially south of *Le Planet*. North of these moraines, another
370 set of latero-frontal moraine relicts deposited by the neighbor Tour Glacier are visible near *Le*
371 *Planet* (Figure 2).

372 **4.2. Moraine and bedrock exposure ages**

373 All ^{10}Be exposure ages are listed in Table 1 and depicted in Figure 7. In the text, individual
374 exposure ages are presented with their 1σ analytical errors; in addition, Table 1 shows the 1σ
375 external errors, including the ^{10}Be production rate error. Before calculating the mean ages of
376 the glacial landforms, each age population was subject to a χ^2 test (2σ) to identify any
377 potential outliers. The landform ages correspond to the arithmetic means of the sample ages
378 and the uncertainties to their standard deviations (in the text and figures for internal
379 comparison); Table 1 also shows the errors that include the ^{10}Be production rate errors.
380 Probability plots of all boulder and moraine mean ages are illustrated in Figure 8.
381 Five samples from *La Joux* area yield ages between 13.2 ± 0.4 ka (LJX-17-5), corresponding
382 to an isolated boulder in front of the outmost moraine (J1), and 9.7 ± 0.3 ka (LJX-17-4),
383 which is the only age from J1 moraine. The mean age for the J2 moraine is 10.9 ± 0.9 ka (n =
384 2), after discarding sample LJX-17-1 (51.9 ± 2.7 ka) as an outlier. This latter boulder surface
385 was most likely affected by isotope inheritance from earlier periods of exposure to cosmic
386 radiation. Ages for the J1 and J2 frontal moraines are not in stratigraphic order, but the J1 age
387 relies upon only one sample, which might have been underestimated due to surface cover by
388 vegetation, erosion or anthropogenic impact, as the *La Joux* area is located in an area covered
389 by forest, close to a village.

390

Sample name	Latitude (dd)	Longitude (dd)	Altitude (masl)	Thickness (mm)	Shielding factor	Quartz weight (g)	Carrier (mg ^{9}Be)	Associated blank	^{10}Be/^{9}Be x10^{-14}	[^{10}Be] (x 10^{4} at.g^{-1})	^{10}Be age (ka)	1σ analytical error (ka)	1σ external error (ka)
LOGNAN AREA													
MORAINE SAMPLE													
L1												11.66 ± 0.70 (0.76)	
ARG-16-9	45.96670	6.96065	2252	26	0.939	26.18	0.2979	30Jan17	35.8 ± 1.7	26.8 ± 1.3	12.21	0.58	0.64
ARG-16-10 (O)	*45.96680*	*6.96056*	*2246*	*32*	*0.939*	*27.08*	*0.2996*	*30Jan17*	*29.9 ± 2.0*	*21.8 ± 1.5*	*10.10*	*0.64*	*0.68*
ARG-16-11	45.96691	6.96050	2239	25	0.950	28.16	0.3008	30Jan17	33.0 ± 1.4	23.3 ± 1.0	10.63	0.42	0.48
ARG-16-12	45.96704	6.96041	2235	40	0.949	28.08	0.3062	30Jan17	35.8 ± 2.1	25.8 ± 1.5	11.88	0.68	0.73
ARG-16-13	45.96744	6.96031	2216	38	0.959	27.79	0.3012	30Jan17	36.1 ± 1.7	25.8 ± 1.2	11.93	0.55	0.61
L2												10.44 ± 0.19 (0.32)	
ARG-16-1	45.96575	6.96317	2287	20	0.970	27.84	0.2996	30Jan17	33.6 ± 2.2	23.8 ± 1.6	10.28	0.66	0.70
ARG-16-2	45.96575	6.96320	2274	50	0.970	27.55	0.2995	30Jan17	32.5 ± 2.1	23.3 ± 1.5	10.39	0.65	0.69
ARG-15-11	45.96551	6.96333	2265	45	0.969	12.75	0.3063	9Mai16	15.27 ± 0.47	23.87 ± 0.77	10.65	0.32	0.40
L3												10.41 ± 0.37 (0.45)	
ARG-16-3	45.96641	6.96312	2255	27	0.973	26.99	0.2993	30Jan17	32.9 ± 1.1	24.03 ± 0.79	10.61	0.33	0.41
ARG-16-4	45.96648	6.96289	2247	35	0.98	26.44	0.2993	30Jan17	31.7 ± 1.0	23.66 ± 0.77	10.52	0.32	0.40
ARG-15-12	45.96686	6.963	2235	22	0.974	18.27	0.3058	9Mai16	22.3 ± 0.7	24.41 ± 0.77	10.87	0.33	0.40

ARG-16-5 (O)	*45.96703*	*6.96292*	*2234*	*20*	*0.971*	*27.98*	*0.3019*	*30Jan17*	*55.8 ± 5.0*	*39.9 ± 3.6*	*17.42*	*1.49*	*1.55*
ARG-16-6	45.96736	6.96278	2216	50	0.971	28.00	0.3001	30Jan17	30.60 ± 0.95	21.60 ± 0.68	10.04	0.30	0.38
ARG-16-7	45.9679	6.96246	2189	30	0.971	28.63	0.3005	30Jan17	31.1 ± 1.1	21.50 ± 0.77	10.01	0.34	0.41
BEDROCK SAMPLE													
ARG-15-5	45.96075	6.96705	2502	30	0.978	18.49	0.312	9Mai16	26.56 ± 0.96	29.6 ± 1.1	11.02	0.37	0.45
ARG-15-6	45.96123	6.96753	2465	20	0.977	9.37	0.3083	9Mai16	15.41 ± 0.57	33.2 ± 1.2	12.50	0.45	0.54
ARG-15-7	45.96181	6.96773	2427	35	0.974	8.09	0.3047	9Mai16	11.42 ± 0.41	27.9 ± 1.0	11.02	0.38	0.46
ARG-16-8	45.96650	6.96061	2384	25	0.485	13.25	0.2965	3Avril17	8.93 ± 0.46	12.86 ± 0.70	10.44	0.53	0.58
ARG-16-14	45.96727	6.96208	2252	28	0.969	20.20	0.2985	3Avril17	22.94 ± 0.96	22.3 ± 1.0	9.97	0.40	0.46
CREMERIE AREA													
C1													
ARG-17-1 (D)	*45.98111*	*6.93959*	*1396*	*22*	*0.954*	*19.71*	*0.3009*	*3Avril17*	*1.79 ± 0.21*	*1.36 ± 0.22*	*1.16*	*0.19*	*0.21*
ARG-17-2	45.98112	6.93975	1399	28	0.952	19.76	0.2903	3Avril17	1.55 ± 0.15	1.07 ± 0.16	0.90	0.14	0.14
ARG-17-3 (D)	*45.98099*	*6.93985*	*1403*	*22*	*0.954*	*20.54*	*0.2817*	*3Avril17*	*1.65 ± 0.28*	*1.07 ± 0.26*	*0.89*	*0.23*	*0.23*
C2													
ARG-17-4 (D)	*45.98070*	*6.93989*	*1407*	*36*	*0.960*	*20.16*	*0.2983*	*3Avril17*	*2.8 ± 3.3*	*2.32 ± 0.33*	*2.04*	*0.31*	*0.31*
ARG-17-5 (D)	*45.98046*	*6.94044*	*1408*	*28*	*0.956*	*20.47*	*0.2515*	*3Avril17*	*4.98 ± 0.47*	*3.64 ± 0.39*	*3.24*	*0.34*	*0.35*

LA JOUX AREA

J2													10.93 ± 0.86 (0.90)
LJX-17-1 (O)	*45.96437*	*6.90778*	*1214*	*24*	*0.955*	*12.01*	*0.2993*	*15Jan18*	*33.2 ± 1.6*	*54.7 ± 2.6*	*51.93*	*2.67*	*2.98*
LJX-17-2	45.96380	6.90743	1216	32	0.955	15.45	0.3091	15Jan18	8.28 ± 0.52	10.61 ± 0.69	10.32	0.64	0.68
LJX-17-3	45.96318	6.90777	1213	41	0.955	23.66	0.3067	15Jan18	13.99 ± 0.53	11.82 ± 0.46	11.53	0.43	0.51
J1													
LJX-17-4	45.96231	6.90604	1215	28	0.955	20.23	0.3007	15Jan18	10.41 ± 0.32	9.99 ± 0.32	9.70	0.30	0.38
LJX-17-5	45.96139	6.90607	1209	48	0.955	21.63	0.3083	15Jan18	14.41 ± 0.45	13.4 ± 4.3	13.17	0.41	0.52

BLANKS	Carrier (mg ^{9}Be)	^{10}Be/^{9}Be x10^{-14}	^{10}Be (x 10^{4} at)
9Mai16	0.3068	0.321 ± 0.046	6.6 ± 1.0
30Jan17	0.3002	0.452 ± 0.057	9.1 ± 1.2
3Avril17	0.2788	0.487 ± 0.073	9.1 ± 1.4
15Jan18	0.3075	0.348 ± 0.050	7.2 ± 1.0

Table 1: Sample [A] and blanks [B] details, analytical data related to ^{10}Be measurements and surface exposure ages. Outliers (O) were determined based on χ2 test (2σ). Mean landform ages are also indicated with standard deviations and total uncertainties in parentheses. Samples from the Crèmerie area have been discarded (D) as the current were <1µA and blank corrections >50%.

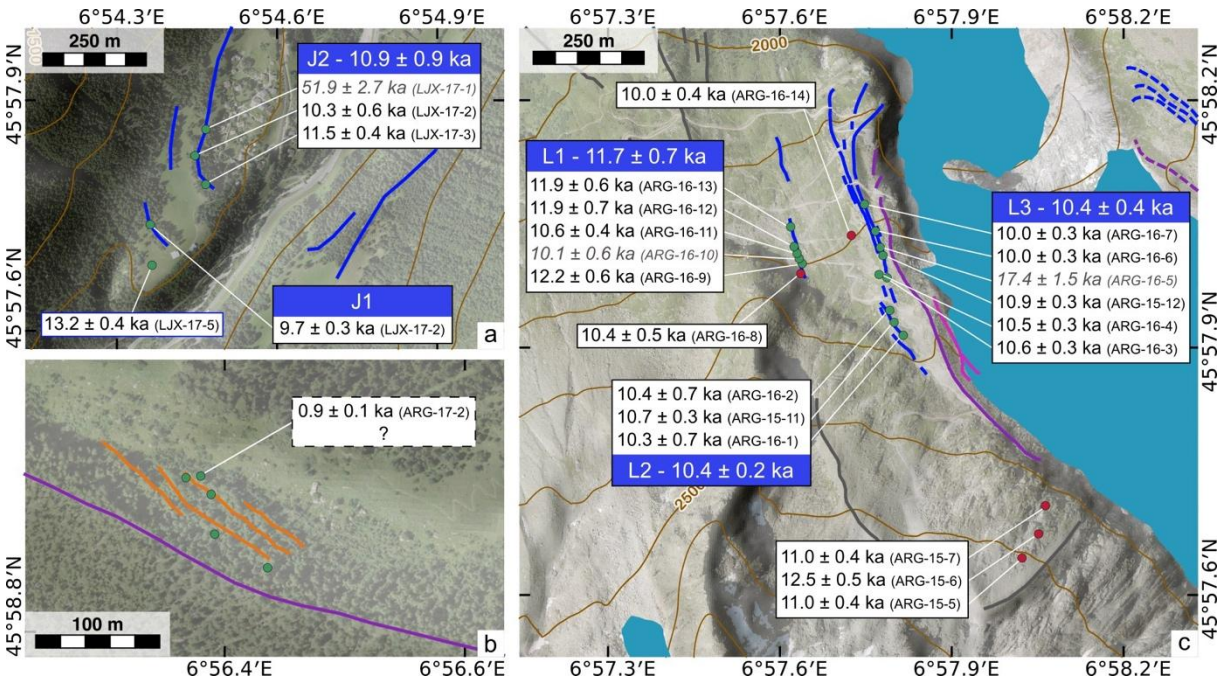

Figure 7: Individual ^{10}Be exposure ages (white boxes) and mean ^{10}Be ages (colored boxes) of glacial landforms (moraines and glacially polished bedrock) in the study areas of the Argentière glacier (a) La Joux, (b) Crèmerie, and (c) Lognan. Red dots represent bedrock samples and green dots boulder samples. Outliers, rejected based on χ^2 statistics, are in italic grey font. Errors of individual ages correspond to the analytical error only. Mean ages are arithmetic means and standard deviation.

In the *Lognan* area, the three bedrock samples taken from roches moutonnées slope between Rognons glacier and Argentière glacier yield ages of 11.0 ± 0.4 (ARG-15-7), 12.5 ± 0.5 (ARG-15-6) and 11.0 ± 0.4 ka (ARG-15-5). From the moraine sequence located directly to the north, we dated three moraines (L1-L3), two of which lie very close together (L2, L3; Figure 7) The outmost one (L1) yields five boulder ages between 12.2 ± 0.6 and 10.6 ± 0.4 ka, with a mean of 11.7 ± 0.7 ka, after discarding ARG-16-10 (10.1 ± 0.6 ka) as an outlier. Three boulders were dated from L2, giving ages between 10.3 ± 0.7 and 10.7 ± 0.3 ka and a mean age of 10.4 ± 0.2 ka. L3 yields five ages between 10.0 ± 0.3 and 10.9 ± 0.3 ka with a mean age of 10.4 ± 0.4 ka, after removing ARG-16-5 (17.4 ± 1.5 ka) as an outlier. These

glacial landform ages are in good stratigraphic order. The similar ^{10}Be ages of the latero-frontal moraines in the *La Joux* area (between ~10.9 ka and 9.7 ka) and of the lateral moraines in the Lognan area (between ~11.7 ka and 10.4 ka) implies that the deposition of these moraines most likely corresponds to the same glacier advances or stillstands.

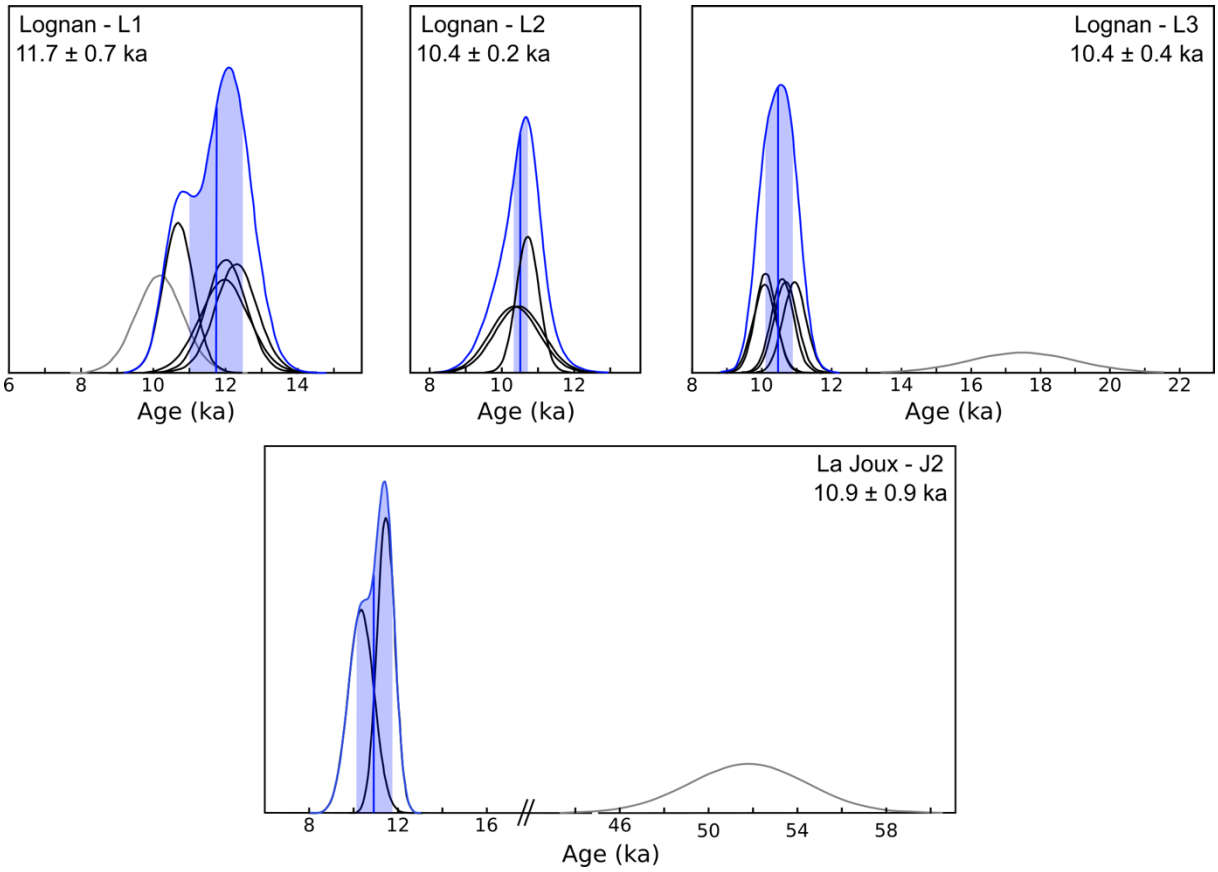

Figure 8 : Summed probability plots (colored curves – colors refer to the legend of Figure 2) of ^{10}Be boulder ages from Argentière glacier. Probability curves of individual ages (black curves) include analytical errors only. Ages indicated in each box are arithmetic means and standard deviations, also visually represented as vertical lines and colored band. Grey curves are outliers.

Two additional bedrock surfaces were sampled next to the Lognan moraines. One on the foot of the bedrock slope at the southern extremity of L1 was dated at 10.4 ± 0.5 ka (ARG-16-8), and another one located between L1 and L3, taken from the flat ground, was dated at 10.0 ± 0.4 ka (ARG-16-14). Even if these two ages are statistically indistinguishable from the mean

ages of the moraines that framed them and the low number of bedrock ages does not allow a robust comparison, they apparently tend to be slightly younger than the moraines. This could be explained by degradation and erosion of the samples (in the case of ARG-16-8) and sediment, vegetation and/or snow cover, in particular for ARG-16-14 as it is on ground level, which in both cases results in an underestimation of the ages.

The batch of the five samples taken in the *Crèmerie* area (C1 and C2 moraines) was subject to a failure during the chemical preparation of the samples, leading to low-quality measurements. Only sample ARG-17-2 from moraine C1 was retained due to sufficiently high ^{9}Be currents (>1 µA) during the AMS measurements, and yielded an age of 0.9 ± 0.2 ka. However, as this is only a single moraine age with high analytical error and therefore does not allow us to reliably interpret the deposition age of the moraines in the *Crèmerie* area, we do not consider it further.

Based on presented ages and on the mapping of all preserved moraines, we reconstruct the extents of the glacier during the YD/EH transition and the Little Ice Age maximum in comparison with that of the year 2008, as shown in Figure 9.

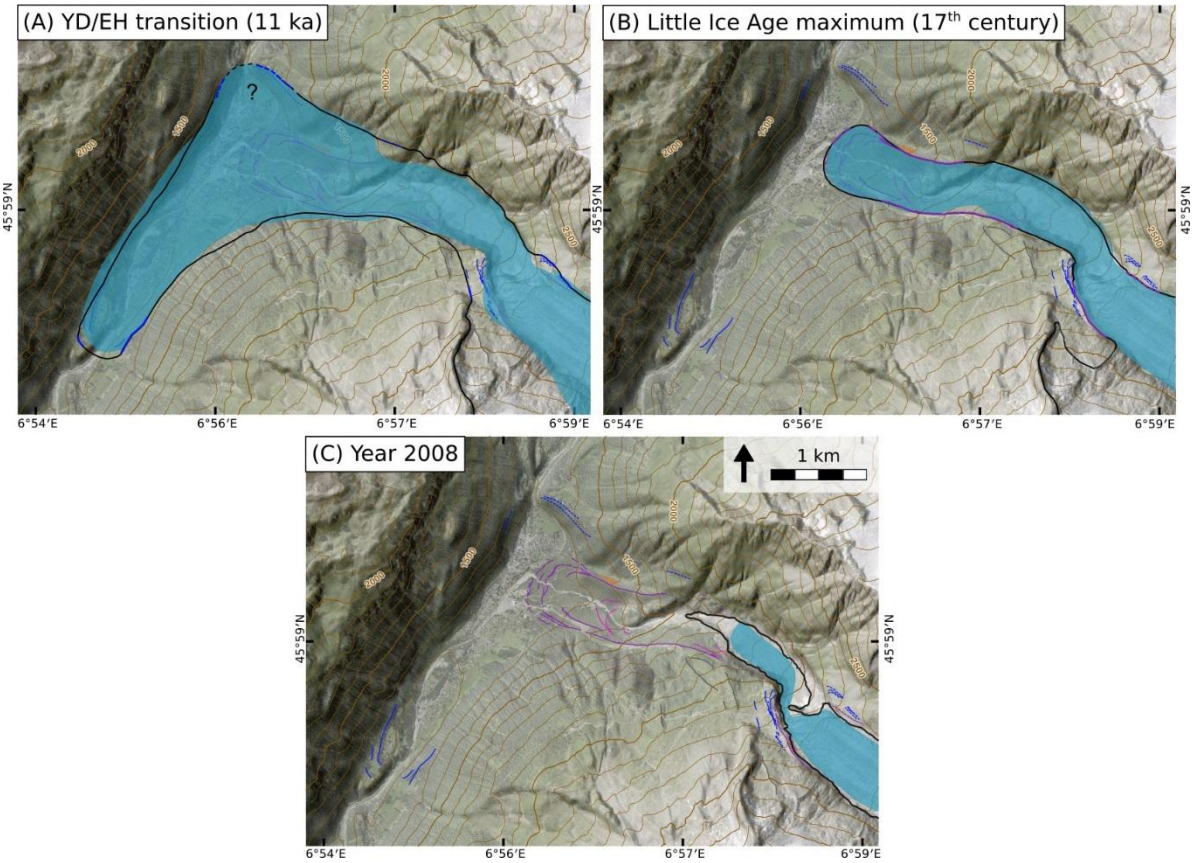

Figure 9 : Black curves represent the reconstruction of past extents of the Argentière glacier, based on mapping of the preserved moraines and interpretation of ^{10}Be dating, for the (A) Younger Dryas/Early Holocene transition (~11 ka - J2 moraines) (B) LIA maximum (17th century) and (C) year 2008. Dashed glacier limits with "?" correspond to hypothetical extents. Blue extensions represent the vertical projection of the 3D reconstruction with the ArcGIS toolbox GlaRe.

4.3. ELA determination

The ELAs resulting from the different methods described in section 3.2 are presented in Table 2. The contours of the ice surface resulting from the 3D reconstructions using the ArcGIS toolbox GlaRe and used for the ELAs calculations are represented in Figure 9 (blue areas).

According to the GIS-based reconstruction method, the ELAs computed for the glacier extent corresponding to the LIA maximum (17th century) and the moraine J2 (~11 ka) using the AABR method are 2738 m and 2523 m a.s.l., respectively. With the AAR method, they are

2753 m and 2648 m a.s.l., respectively. The ELA rise between the two extents is of 215 m with the AABR method, while it is 105 m with the AAR method. The modeling of the same extents using the PDD model, assuming the same precipitation as today, leads to ELA values of 2753 m for the 17th century and 2442 m a.s.l. for the ~11 ka period. The associated ELA rise between the two extents is 311 m.

	ELA (m a.s.l.)			ΔELA (m)		
	present	LIA	~11 ka (J2 moraine)	LIA - present	~11 ka - present	11 ka - LIA
AABR	2866	2738	2523	128	343	215
AAR	2801	2753	2648	48	153	105
PDD	2940	2753	2442	187	498	311

Table 2: Comparison of ELA calculations using the AABR and AAR methods and the PDD modeling for Argentière glacier for the present-day (i.e. year 2008 for the AABR and AAR methods and 1979-2002 for the PDD modeling), the LIA maximum (17th century) and the J2 moraine (~11 ka; YD/EH transition). For the AABR method a Balance ratio of 1.59 (Rea, 2009) is used and for the AAR method a ratio of 0.67 (Gross et al., 1977), both representative for the Alps. For the PDD model, ELA values are inferred with the same precipitation condition as today.

4.4. Paleoclimatic results

4.4.1. Temperature results from the GIS-based reconstructions

The temperature differences inferred from the GIS-based ELA reconstructions (AABR and AAR methods) between ~11 ka, the LIA maximum (17th century) and the year 2008 are presented in Table 3. The 128-m rise of the ELA between the LIA maximum and the year 2008 inferred from the AABR method is equivalent to a +1.1°C difference in summer temperature, according to the ELA sensitivity to summer temperature of 115 m°C^{-1} (Rabatel et al., 2013). Using the local ELA sensitivity of 72 m°C^{-1} (Six and Vincent, 2014), it is +1.8°C. The temperature difference between ~11 ka and the year 2008 (ELA-rise of 331 m),

using the same two ELA temperature-sensitivity values as above, is +3°C and +4.8°C, respectively.

For the sake of comparison with other studies from the Alps, we also give the results from the AAR method, noting that the ELA-rise is traditionally estimated with reference to the LIA maximum glacier extent. According to this approach, our reconstruction leads to an ELA-rise between ~11 ka and the LIA maximum of 105 m, which corresponds to +0.9°C and +1.4°C, respectively. Between ~11 ka and 2008, this approach gives a difference of +1.3°C and +2.1°C, respectively, equivalent to an ELA rise of 153 m. And between the LIA maximum and 2008, the ELA-rise is 48 m, corresponding to a temperature difference of +0.4°C and +0.7°C, respectively. These latter results seem to be underestimated when comparing them to the values inferred from the measurements at the beginning of the 19th century (~+1.0°C; Auer et al., 2007; Figure 5), a period when the glacier was even slightly smaller than during the 17th century. On the other hand, the temperature results from the AABR method (+1.1°C/+1.8°C) are coherent with the instrumental data.

	ΔT [LIA - year 2008] (°C)		ΔT [~11 ka - year 2008] (°C)		ΔT [~11 ka - LIA] (°C)	
AABR	+1.1	+1.8	+3.0	+4.8	+1.8	+2.9
AAR	+0.4	+0.7	+1.3	+2.1	+0.9	+1.4

Table 3: Comparison of the temperature differences inferred from the ΔELA calculated from the AABR and AAR methods (presented in Table 2) using two different ELA sensitivity to temperature: 115 m°C^{-1} (Rabatel et al., 2013) on the left and 72 m°C^{-1} (Six and Vincent, 2014) on the right. LIA refers to the LIA maximum (17th century).

4.4.2. Paleoclimatic results from the PDD modeling

Applying the PDD modeling approach, we determined the potential combinations of precipitation and temperature conditions corresponding to each investigated glacier extent. The glacier extents at four different dates were investigated (see Figure 2 to visualize the extents): the years 1850 and 1820, for which the glacier extents and regional climate

conditions are well known, the 17th century (LIA maximum) and the extent at ~11 ka using the moraine J2 as the frontal limit. The modeling gives an infinite number of combinations of temperature and precipitation conditions that explain the frontal moraine position at the four investigated dates. The curves in Figure 10 represent these combinations, considering temperatures between 0°C and 8°C below that of the reference period (1979-2002) and precipitation amounts between 0 and 2 times that of the reference period. This figure also shows the range of ELAs resulting from the model for each of the four glacier extents. The ELAs increase with precipitation.

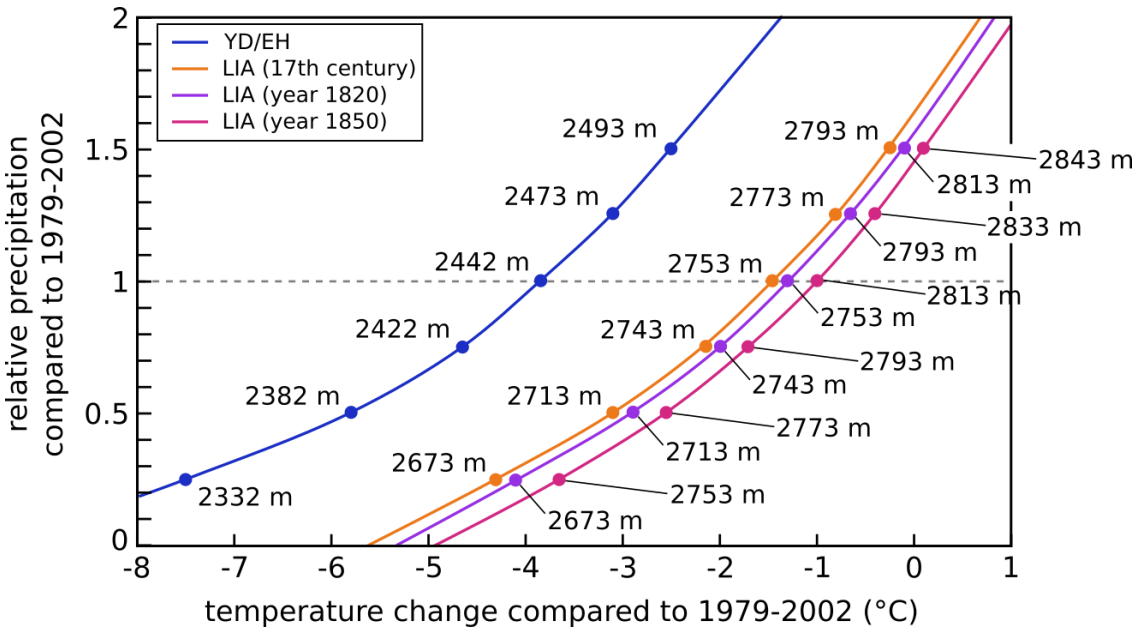

Figure 10 : Paleoclimatic reconstructions of the Argentière glacier for the YD/EH transition (blue) and the 17th century (orange), 1820 (purple) and 1850. (pink) glacier extent. Temperature changes, with respect to the 1979-2002 period, are plotted against relative precipitation amount normalized to the 1979-2002 period. One curve reflects all combinations of temperature and precipitation for one glacier extent (constrained by the frontal moraines). The altitudes refer to the ELA associated with each temperature-precipitation couple.

Climate influence on Argentière glacier is explored through modeling of its extents at the end of the LIA, when climatic evolution is already instrumentally recorded. As the instrumental climatic data used for comparison with our results do not cover the 17th century, only the results of 1850 and 1820 are subject to discussions of the LIA paleoclimate. Based on the data collected in the HISTALP project (http://www.zamg.ac.at/histalp/; Auer et al., 2007), we estimate the annual temperature for the years 1850 and 1820. We then deduce the precipitation, which is more likely to vary locally, from the PDD model. All values are calculated relative to the 1979-2002 period, which is the "present-day" reference period used in the PDD model (see section 3.2). A shift of 10-14 years between the extraction of the temperature value and the date of the studied extent has been applied in order to take into account the glacier's response time (Vincent et al., 2009). The measured temperature differences compared to the period of reference are around -1.4°C for 1850 and around -1.0°C for 1820 (Figure 5). Thus, colder conditions prevailed when the glacier was shorter, in 1850. According to these temperature differences and the temperature-precipitation relationships in Figure 11, precipitation amounts were lower by ~15% in 1850 and higher by ~10% in 1820 compared to the 1979-2002 average. If the temperatures had been inferred from our PDD model assuming the same amount of precipitation as in 1979-2002, the 1850 temperature would have been overestimated by ~0.4°C and the 1820 temperature underestimated by ~0.2°C.

Constraining a unique temperature/precipitation couple for the ~11 ka glacier extent is much more challenging due to the scarcity and uncertainties of pure paleo-precipitation and paleo-temperature records for this time in the Alps. Therefore, we use the following rationales to narrow down the potential range of precipitation/temperature couples. As moraines are only built below the ELA (e.g. Anderson and Anderson, 2010) and the maximal elevation of the moraine sequence corresponding to the YD/EH transition on the glacier bank opposite to the

Lognan area is ~2400 m a.s.l. (Figure 2), the ELA during this period was at least as high as 2400 m. This observation allows us to limit the temperature difference compared to 1979-2002 to -5.5°C (lower bound) and to a minimum of 45% of the 1979-2002 averaged precipitation amount (Figure 10 and Figure 11). Then, assuming that the amount of precipitation was not superior to that during the end of the LIA, i.e. up to 10% precipitation more than during the 1979-2002 period, the upper temperature limit is at -3.6°C. The temperature values of -3°C and -4.8°C, inferred above from the GIS based estimations (AABR method) for the same glacier extent, compare well with these temperature bounds of -5.5°C and -3.6°C resulting from the PDD model, supporting the findings from both methods. The relatively high potential temperature ranges reflect the uncertainty arising from the choice of the value for the ELA sensitivity to temperature in the first approach and from the range of possible precipitation amounts in the second approach.

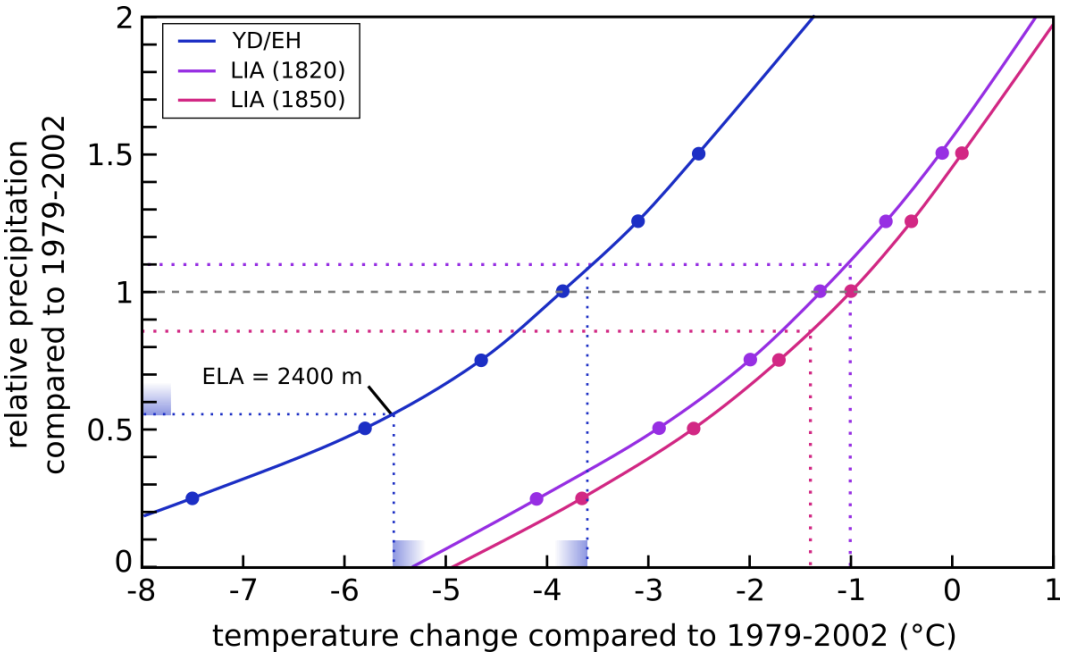

Figure 11 : Same as Fig. 10, but for the YD/EH transition (blue), 1820 (purple) and 1850 (pink) glacier extent only, with marks of the paleoclimatic interpretations.

5 Discussion

5.1. Holocene oscillations of Argentière glacier

As outlined in section 2, numerous glacio-geomorphic markers in the Arve valley attest to the glacier extents during the LGM and to various advances or stillstands during the deglaciation of the Late-glacial. The moraine ages from the La Joux and Lognan areas are younger than 11.7 ka and therefore fall into the Early Holocene, apart from L1 moraine, which overlaps with the Younger Dryas within uncertainties. The ^{10}Be ages of the three roche moutonnée samples located between Rognons and Argentière glacier (11.0 ± 0.4 ka, 12.5 ± 0.4 ka, 11.0 ± 0.4 ka) and of the Lognan bedrock surfaces (10.4 ± 0.5 ka and 10.0 ± 0.4 ka) suggest that the general deglaciation of this area occurred during the YD/EH transition. These ages are statistically the same as the ^{10}Be mean ages of moraines L1, L2 and L3 (11.7 ± 0.7 ka, 10.4 ± 0.2 ka and 10.4 ± 0.4 ka) in the Lognan area, indicating that the deglaciation process was shortly interrupted by glacier stillstands or re-advances. The isolated bloc dated at 13.2 ± 0.4 ka in front of the J1 moraine in the *La Joux* area tentatively suggests that the front of the glacier may already have retreated to a similar position as moraines J1 and J2 ~2 ka before the YD/EH transition, but this scenario would need more evidence to be confirmed. The existence of at least five morainic ridges between L1 and L3 (Figure 7C) indicate that Argentière glacier stagnated or re-advanced at least five times between ~11.7 and ~10.4 ka ago. These results from the lateral moraines in the Lognan area are coherent with the observations in the frontal area of *La Joux*, where at least three preserved ridges of Early Holocene age (~11 ka) can be distinguished (among them J1 and J2). The similarity of the moraine and bedrock ages as well as the smooth and low morphology of the moraines suggest that the glacier did not retreat far up-valley between the moments of moraine deposition and that these moraines correspond to periods of glacier stillstands during the deglaciation rather than to massive re-advances. Finally, the innermost moraine ages and the bedrock ages in the Lognan area imply that the glacier definitively retreated from its Early Holocene extent at ~10.4 ka ago.

Further evidence of advanced extents of Argentière glacier during the Late Holocene comes from the study by Bless (1984) who suggested five advances of Argentière glacier between ~4 ka and ~1.2 ka, based on radiocarbon-dated subfossil wood found in the right-lateral moraine outcrop (location in Figure 2). Multiple advances during this period were also reported for other glaciers in the Mont-Blanc massif (e.g. Deline and Orombelli, 2005; Le Roy et al., 2015). In particular, the numerous dendrochronologically-dated advances of the neighbor Mer de Glace between ~3.5 ka and 0.7 ka ago (Le Roy et al. (2015); location in Figure 1), support the hypothesis of Late Holocene advances of Argentière glacier. However, considering that so far none of the preserved and dated moraines gave a Late Holocene age that pre-dates the LIA, we assume that the Late Holocene extents of Argentière glacier were smaller than those during the LIA maximum.

5.2. Paleoclimatic interpretations

5.2.1. Comparison with previously glacier-derived paleoclimate reconstructions from Argentière glacier and other sites in the Alps

The results of the PDD modeling for the 1820 and 1850 extents indicate that precipitation was higher in 1820 than in 1850. Regionally higher precipitation in 1820 was also recorded in the western part of the Alps according to the HISTALP annual precipitation time series (Figure 5), but the difference in precipitation amount between 1850 and 1820 is only of ~10%, against ~20% according to our modeling. Our results are consistent with the conclusions from previous PDD modeling of Argentière glacier (Vincent et al., 2005), which explains observed glacier advances during the period 1760-1830 with winter precipitations higher by at least 25% than the 20th century average, while summer temperature had not decreased. They also attribute the subsequent retreat of the glacier to a decrease in winter precipitation. Even if our findings are not directly comparable, as our modelling only allows us to consider the annual and not the seasonal climate variations and Vincent et al. (2005) based their model on less

cooling than we do here, we can still notice that the trend is the same, i.e. higher precipitation in 1820 compared to 1850 explains the bigger glacier extent. Given that the 19th century maximum of bigger glaciers in the Swiss Alps occurred in 1850-1860 rather than in 1820 (Holzhauser et al., 2005), the glacier size and local variations in precipitations during the LIA could explain the detailed differences in the behavior of Argentière glacier compared to smaller glaciers in other Alpine regions. These results illustrate that ignoring the role of precipitation might lead to a first-order approximation of past temperature conditions. Our results also show that the impact of local precipitation variations on mountain glacier dynamics superimposes on those of large scale temperature variations and can thus explain the local differences in the behavior of glaciers from different parts of a massif, like the Alps, and the small fluctuations of a glacier during one glacial stadial, like the LIA.

Temperature reconstructions for the YD/EH transition using the AAR method have previously been performed at glacier sites in the Alps. Moran et al. (2016) reconstructed from the extents of two glaciers in the Eastern Alps that summer temperatures were 1.5°C lower during the YD/EH transition than in the mid 20th century, which is in good agreement with the difference of 1.3°C/2.1°C inferred from the extents of Argentière glacier during the YD/EH transition and the year 2008 when using the AAR method. These results are also coherent with the findings of Hofmann et al. (2019) who inferred a temperature difference of 1.5°C between the YD/EH transition and the LIA in the westernmost French Alps. Nonetheless, due to the extremely simplified assumptions on the glacier geometry of the AAR method (section 3.3.1), we believe that temperature reconstructions based on this approach should be taken with caution. The coherence between the relative temperature reconstructed from the local LIA maximum glacier extent and the one measured at the end of the LIA (section 4.4.1) makes us indeed confident that the AABR method is more reliable than the AAR method when inferring paleotemperatures from ELA reconstructions.

5.2.2. Comparison with paleoclimate results from independent proxy records

Comparison of our precipitation range assumptions for the YD/EH transition (-45% to +10% of the present precipitation amount) with independent proxy records is difficult. Given that precipitation can significantly vary locally, it would be ideal to consider a local precipitation estimate in or near the Mont-Blanc massif for this period. However, to our knowledge this does not exist. The complexity of the precipitation variability during the Younger Dryas and the Early Holocene has indeed been underlined by Magny et al. (2001). Recent global climate simulations combined with proxy-based temperature reconstructions suggest that the Younger Dryas was considerably drier and the Early Holocene was less dry in Central Europe than the preceding Allerod period (Renssen et al., 2018), but no quantification of the precipitation conditions relative to the present is available.

Alpine and European temperature reconstructions for the Younger Dryas and Early Holocene based on independent proxies are more frequent. However, the range of reconstructed annual and summer temperatures for the Younger Dryas is large, it varies from 6 to 2°C below modern values when inferred from records of pollen and cladocera assemblages from Gerzensee in the North-alpine foreland in Switzerland (Lotter et al., 2000), investigation of stalagmites in Hölloch cave in the German Alps (Wurth et al., 2004) or chironomid records from a paleolake in the Central Swiss Alps (Ilyashuk et al., 2009). Based on high-resolution oxygen isotope records, the beginning of the Holocene is associated with an abrupt temperature rise on regional and hemispheric scale (Alley, 2000; Schwander et al., 2000). Early Holocene temperature reconstructions in the region of the Alps yield, similar to those for the Younger Dryas, a large range of values depending on the used proxy. For example, the chironomid record in the Swiss central Alps indicates ~1-4°C *above* the present July air temperatures for the very beginning of the Holocene (Ilyashuk et al., 2009), while a second chironomid record, also from the Swiss Alps, indicates ~1-1.5°C *below* it (Heiri et al., 2003).

Reconstruction from pollen data indicates an annual anomaly relative to the present of as low as -4.5°C (around 12-11 ka) for the central-western part of Europe (Davis et al., 2003) and summer temperatures of 4.5-5°C below those of the present at Gerzensee (Lotter et al., 2000). The temperature range inferred for the YD/EH transition from our PDD modeling of -5.5°C to -3.6°C and from the ELA reconstruction with the AABR method of -4.8°C/-3.0°C, agrees with the coldest results from alpine proxy records for this period (e.g. Davis et al., 2003; Lotter et al., 2000), reinforcing our results for the western Alps.

However, the large divergence between the paleo-temperature reconstructions depending on the method and parameters used highlights that further investigations are necessary to refine methods that aim at inferring paleo-climate conditions from past glacier extents and to complete the here presented findings.

6. Conclusions

Our new Holocene chronology for the Argentière glacier based on 29 cosmogenic ^{10}Be cosmogenic dates of moraines and bedrock suggests that Argentière glacier retreated from its large Late-Glacial extent during the Younger Dryas/Early Holocene transition, around 11.7 ka, and that this retreat was interrupted by several stillstands during ~1 ka, followed at ~10.4 by the final glacier retreat to within the LIA limits. We do not have any evidence of glacial advances until the Late Holocene.

Climate reconstruction corresponding to two different glacier extents during the LIA, using a PDD model coupled with a dynamic ice flow model, highlights the influence of local precipitation changes, superimposed on the dominant impact of temperature, on the detailed glacial fluctuations of Argentière glacier. This suggests that disregarding the role of precipitation might lead to first-order temperature approximations when reconstruction paleo-climate conditions from past glacier extents.

The reconstruction of the climatic conditions corresponding to the YD/EH transition extent of the glacier using the PDD model and a simpler approach that only considers the impact of summer temperature on the reconstructed ELAs yield comparable results. The results from the PDD model suggests a temperature difference range of -5.5°C to -3.6°C compared to the present-day period (1979-2002). This agrees with earlier paleoclimate reconstructions from pollen records for the same period, but seems to be quite cold in comparison with the results from other proxy studies and another simple approach of glacier-based temperature reconstruction. The large differences in temperature reconstructions from the various paleoclimate studies and the scarcity of paleo-precipitation records for the Younger Dryas and the Early Holocene highlight the need of additional efforts in investigating the paleoclimatic conditions for these periods.

Acknowledgements

This study is part of ANR project 14-CE03-0006 *VIP Mont-Blanc*. We thank Laëtitia Léanni (CEREGE) for support during sample chemistry, Pierre Jégot and Jules Fleury (CEREGE) for help during ELA determination and Daniel Joly and Benjamin Pohl for sharing temperature and precipitation data. The 2015 DEM of Argentière glacier catchment has been acquired within the project ISOTHERM led by Antoine Rabatel (Univ. Grenoble Alpes, IGE) founded by EUFAR (EUropean Facility for Airborne Research). We also thank the IRSTEA for the Arve valley DEM. The ASTER AMS national facility (CEREGE) is supported by the INSU/CNRS, the ANR through the "projet thématiques d'excellence" program for the "Equipements d'excellence" ASTER-CEREGE action and IRD. We thank Benjamin Chandler and one anonymous reviewer whose relevant remarks have helped to improve this manuscript.

References

Alley, R.B., 2000. The Younger Dryas cold interval as viewed from central Greenland. Quat. Sci. Rev. 19, 213–226. https://doi.org/10.1016/S0277-3791(99)00062-1

Anderson, R.S., Anderson, S.P., 2010. Geomorphology: The Mechanics and Chemistry of Landscapes. 2010. Cambridge University Press, 340 pp.

André, M., 2002. Rates of postglacial rock weathering on glacially scoured outcrops (abisko–riksgränsen area, 68°n). Geogr. Ann. Ser. Phys. Geogr. 84, 139–150. https://doi.org/10.1111/j.0435-3676.2002.00168.x

Arnold, M., Merchel, S., Bourlès, D.L., Braucher, R., Benedetti, L., Finkel, R.C., Aumaître, G., Gottdang, A., Klein, M., 2010. The French accelerator mass spectrometry facility ASTER: Improved performance and developments. Nucl. Instrum. Methods Phys. Res. Sect. B Beam Interact. Mater. At., 19th International Conference on Ion Beam Analysis 268, 1954–1959. https://doi.org/10.1016/j.nimb.2010.02.107

Auer, I., Böhm, R., Jurkovic, A., Lipa, W., Orlik, A., Potzmann, R., Schöner, W., Ungersböck, M., Matulla, C., Briffa, K., Jones, P., Efthymiadis, D., Brunetti, M., Nanni, T., Maugeri, M., Mercalli, L., Mestre, O., Moisselin, J.-M., Begert, M., Müller-Westermeier, G., Kveton, V., Bochnicek, O., Stastny, P., Lapin, M., Szalai, S., Szentimrey, T., Cegnar, T., Dolinar, M., Gajic-Capka, M., Zaninovic, K., Majstorovic, Z., Nieplova, E., 2007. HISTALP—historical instrumental climatological surface time series of the Greater Alpine Region. Int. J. Climatol. 27, 17–46. https://doi.org/10.1002/joc.1377

Balco, G., Briner, J., Finkel, R.C., Rayburn, J.A., Ridge, J.C., Schaefer, J.M., 2009. Regional beryllium-10 production rate calibration for late-glacial northeastern North America. Quat. Geochronol. 4, 93–107. https://doi.org/10.1016/j.quageo.2008.09.001

Baroni, C., Casale, S., Salvatore, M.C., Ivy-Ochs, S., Christl, M., Carturan, L., Seppi, R., Carton, A., 2017. Double response of glaciers in the Upper Peio Valley (Rhaetian Alps, Italy) to the Younger Dryas climatic deterioration. Boreas 46, 783–798. https://doi.org/10.1111/bor.12284

Benn, D.I., Lehmkuhl, F., 2000. Mass balance and equilibrium-line altitudes of glaciers in high-mountain environments. Quat. Int. 65–66, 15–29. https://doi.org/10.1016/S1040-6182(99)00034-8

Biette, M., Jomelli, V., Favier, V., Chenet, M., Agosta, C., Fettweis, X., Minh, D.H.T., Ose, K., 2018. Estimation des températures au début du dernier millénaire dans l'ouest du Groenland : résultats préliminaires issus de l'application d'un modèle glaciologique de type

735 degré- jour sur le glacier du Lyngmarksbræen. Géomorphologie Relief Process. Environ. 24.
736 https://doi.org/10.4000/geomorphologie.11977
737 Blard, P.-H., Lavé, J., Pik, R., Wagnon, P., Bourlès, D., 2007. Persistence of full glacial
738 conditions in the central Pacific until 15,000 years ago. Nature 449, 591–594.
739 https://doi.org/10.1038/nature06142
740 Bless, R., 1984. Beträge zur Spät und Postglazialen Geschichte der Gletscher im
741 Nordöstlichen Mont Blanc Gebiet. Phys. Geogr. 15.
742 Braucher, R., Guillou, V., Bourlès, D.L., Arnold, M., Aumaître, G., Keddadouche, K.,
743 Nottoli, E., 2015. Preparation of ASTER in-house 10Be/9Be standard solutions. Nucl.
744 Instrum. Methods Phys. Res. Sect. B Beam Interact. Mater. At., The Thirteenth Accelerator
745 Mass Spectrometry Conference 361, 335–340. https://doi.org/10.1016/j.nimb.2015.06.012
746 Bussy, F., Hernandez, J., Raumer, J.V., 2000. Bimodal magmatism as a consequence of the
747 post-collisional readjustment of the thickened Variscan continental lithosphere (Aiguilles
748 Rouges-Mont Blanc Massifs, Western Alps). Earth Environ. Sci. Trans. R. Soc. Edinb. 91,
749 221–233. https://doi.org/10.1017/S0263593300007392
750 Chenet, M., Brunstein, D., Jomelli, V., Roussel, E., Rinterknecht, V., Mokadem, F., Biette,
751 M., Robert, V., Léanni, L., 2016. 10Be cosmic-ray exposure dating of moraines and rock
752 avalanches in the Upper Romanche valley (French Alps): Evidence of two glacial advances
753 during the Late Glacial/Holocene transition. Quat. Sci. Rev. 148, 209–221.
754 https://doi.org/10.1016/j.quascirev.2016.07.025
755 Chmeleff, J., von Blanckenburg, F., Kossert, K., Jakob, D., 2010. Determination of the 10Be
756 half-life by multicollector ICP-MS and liquid scintillation counting. Nucl. Instrum. Methods
757 Phys. Res. Sect. B Beam Interact. Mater. At. 268, 192–199.
758 https://doi.org/10.1016/j.nimb.2009.09.012
759 Claude, A., Ivy-Ochs, S., Kober, F., Antognini, M., Salcher, B., Kubik, P.W., 2014. The
760 Chironico landslide (Valle Leventina, southern Swiss Alps): age and evolution. Swiss J.
761 Geosci. 107, 273–291. https://doi.org/10.1007/s00015-014-0170-z
762 Corbel, J., 1963. Glaciers et climats dans le massif du Mont-Blanc. Rev. Géographie Alp. 51,
763 321–360. https://doi.org/10.3406/rga.1963.3132
764 Coutterand, S., Buoncristiani, J.-F., 2006. Paléogéographie du dernier maximum glaciaire du
765 Pléistocène récent de la région du Massif du Mont Blanc, France. Quat. Rev. Assoc. Fr. Pour
766 Létude Quat. 35–43. https://doi.org/10.4000/quaternaire.633
767 Coutterand, S., Nicoud, G., 2005. Les stades de retrait du glacier de l'Arve entre le verrou de
768 cluses et l'ombilic de Chamonix au cours du Tardiglaciaire (Vallée de l'Arve, Haute-Savoie).

769 Quaternaire 85–94. https://doi.org/10.4000/quaternaire.296
770 Davis, B.A.S., Brewer, S., Stevenson, A.C., Guiot, J., 2003. The temperature of Europe
771 during the Holocene reconstructed from pollen data. Quat. Sci. Rev. 22, 1701–1716.
772 https://doi.org/10.1016/S0277-3791(03)00173-2
773 Deline, P., Orombelli, G., 2005. Glacier fluctuations in the western Alps during the
774 Neoglacial, as indicated by the Miage morainic amphitheatre (Mont Blanc massif, Italy).
775 Boreas 34, 456–467. https://doi.org/10.1080/03009480500231369
776 Fischer, M., Huss, M., Barboux, C., Hoelzle, M., 2014. The New Swiss Glacier Inventory
777 SGI2010: Relevance of Using High-Resolution Source Data in Areas Dominated by Very
778 Small Glaciers. Arct. Antarct. Alp. Res. 46, 933–945. https://doi.org/10.1657/1938-4246-
779 46.4.933
780 Fontaine, R., 2015. Chamonix et ses glaciers : Les premières images sous l'oeil des
781 photographes (1849-1869), Atelier Esope. ed.
782 Francou, B., Vincent, C., 2007. Les glaciers à l'épreuve du climat, Edition IRD. ed.
783 Gardent, M., Rabatel, A., Dedieu, J.-P., Deline, P., 2014. Multitemporal glacier inventory of
784 the French Alps from the late 1960s to the late 2000s. Glob. Planet. Change 120, 24–37.
785 https://doi.org/10.1016/j.gloplacha.2014.05.004
786 Gross, G., Kerschner, H., Patzelt, G., 1977. Methodische Untersuchungen über
787 dieSchneegrenze in alpinen Gletschergebieten. Gletsch Glazialgeol 223–251.
788 Heiri, O., Lotter, A.F., Hausmann, S., Kienast, F., 2003. A chironomid-based Holocene
789 summer air temperature reconstruction from the Swiss Alps. The Holocene 13,
790 477–484. https://doi.org/10.1191/0959683603hl640ft
791 Hofmann, F.M., Alexanderson, H., Schoeneich, P., Mertes, J.R., Léanni, L., Aster Team
792 (Georges Aumaître, Didier L. Bourlès, Karim Keddadouche), 2019. Post-Last Glacial
793 Maximum glacier fluctuations in the southern Écrins massif (westernmost Alps): insights
794 from ^{10}Be cosmic ray exposure dating. Boreas. https://doi.org/10.1111/bor.12405
795 Holzhauser, H., Magny, M., Zumbuühl, H.J., 2005. Glacier and lake-level variations in west-
796 central Europe over the last 3500 years. The Holocene 15, 789–801.
797 https://doi.org/10.1191/0959683605hl853ra
798 Ilyashuk, B., Gobet, E., Heiri, O., Lotter, A.F., van Leeuwen, J.F.N., van der Knaap, W.O.,
799 Ilyashuk, E., Oberli, F., Ammann, B., 2009. Lateglacial environmental and climatic changes
800 at the Maloja Pass, Central Swiss Alps, as recorded by chironomids and pollen. Quat. Sci.
801 Rev. 28, 1340–1353. https://doi.org/10.1016/j.quascirev.2009.01.007
802 Jaillet, S., Ballandras, S., 1999. La transition Tardiglaciaire/Holocène à travers les

fluctuations du glacier du Tour (Vallée de Chamonix, Alpes du Nord françaises) [Lateglacial/Holocene transition through glacier du Tour fluctuations (upper Chamonix valley, French Alps)]. Quaternaire 10, 15–23. https://doi.org/10.3406/quate.1999.1625

Joly, D., Berger, A., Buoncristiani, J.-F., Champagne, O., Pergaud, J., Richard, Y., Soare, P., Pohl, B., 2018. Geomatic downscaling of temperatures in the Mont Blanc massif: A NEW STATISTICAL DOWNSCALING APPROACH. Int. J. Climatol. 38, 1846–1863. https://doi.org/10.1002/joc.5300

Jomelli, V., Khodri, M., Favier, V., Brunstein, D., Ledru, M.-P., Wagnon, P., Blard, P.-H., Sicart, J.-E., Braucher, R., Grancher, D., Bourlès, D.L., Braconnot, P., Vuille, M., 2011. Irregular tropical glacier retreat over the Holocene epoch driven by progressive warming. Nature 474, 196–199. https://doi.org/10.1038/nature10150

Keeler, D.G., 2015. Development and Validation of a Physically Based ELA Model and its Application to the Younger Dryas Event in the Graubünden Alps, Switzerland 70.

Kerschner, H., Ivy-Ochs, S., 2007. Palaeoclimate from glaciers: Examples from the Eastern Alps during the Alpine Lateglacial and early Holocene. Glob. Planet. Change 60, 58–71. https://doi.org/10.1016/j.gloplacha.2006.07.034

Korschinek, G., Bergmaier, A., Faestermann, T., Gerstmann, U.C., Knie, K., Rugel, G., Wallner, A., Dillmann, I., Dollinger, G., von Gostomski, Ch.L., Kossert, K., Maiti, M., Poutivtsev, M., Remmert, A., 2010. A new value for the half-life of 10Be by Heavy-Ion Elastic Recoil Detection and liquid scintillation counting. Nucl. Instrum. Methods Phys. Res. Sect. B Beam Interact. Mater. At. 268, 187–191. https://doi.org/10.1016/j.nimb.2009.09.020

Le Roy, M., 2012. Reconstitution des fluctuations glaciaires holocènes dans les Alpes occidentales : apports de la dendrochronologie et de la datation par isotopes cosmogéniques produits in situ (phdthesis). Université Grenoble Alpes.

Le Roy, M., Deline, P., Carcaillet, J., Schimmelpfennig, I., Ermini, M., 2017. 10Be exposure dating of the timing of Neoglacial glacier advances in the Ecrins-Pelvoux massif, southern French Alps. Quat. Sci. Rev. 178, 118–138. https://doi.org/10.1016/j.quascirev.2017.10.010

Le Roy, M., Nicolussi, K., Deline, P., Astrade, L., Edouard, J.-L., Miramont, C., Arnaud, F., 2015. Calendar-dated glacier variations in the western European Alps during the Neoglacial: the Mer de Glace record, Mont Blanc massif. Quat. Sci. Rev. 108, 1–22. https://doi.org/10.1016/j.quascirev.2014.10.033

Leclercq, P.W., Oerlemans, J., Basagic, H.J., Bushueva, I., Cook, A.J., Le Bris, R., 2014. A data set of worldwide glacier length fluctuations. The Cryosphere 8, 659–672. https://doi.org/10.5194/tc-8-659-2014

Lotter, A.F., Birks, H.J.B., Eicher, U., Hofmann, W., Schwander, J., Wick, L., 2000. Younger Dryas and Allerød summer temperatures at Gerzensee (Switzerland) inferred from fossil pollen and cladoceran assemblages. Palaeogeogr. Palaeoclimatol. Palaeoecol. 159, 349–361. https://doi.org/10.1016/S0031-0182(00)00093-6

Lucéna, S., Ballandras, S., 1999. Rythme des fluctuations glaciaires et détritisme alluvial postglaciaire dans la haute vallée de l'Arve (Alpes françaises du Nord) [Glacial fluctuations rythm and postglacial alluvial detritism in high Arve valley (French North Alps)]. Quaternaire 10, 25–36. https://doi.org/10.3406/quate.1999.1626

Lukas, S., 2007. Early-Holocene glacier fluctuations in Krundalen, south central Norway: palaeoglacier dynamics and palaeoclimate. The Holocene 17, 585–598. https://doi.org/10.1177/0959683607078983

Magny, M., Guiot, J., Schoellammer, P., 2001. Quantitative Reconstruction of Younger Dryas to Mid-Holocene Paleoclimates at Le Locle, Swiss Jura, Using Pollen and Lake-Level Data. Quat. Res. 56, 170–180. https://doi.org/10.1006/qres.2001.2257

Maisch, M., 1981. Glazialmorphologische und gletschergeschichtliche Untersuchungen im Gebiet zwischen Landwasser- und Albulatal (Kt. Graubünden, Schweiz).

Marcott, S.A., Shakun, J.D., Clark, P.U., Mix, A.C., 2013. A Reconstruction of Regional and Global Temperature for the Past 11,300 Years. Science 339, 1198–1201. https://doi.org/10.1126/science.1228026

Martin, L.C.P., Blard, P.-H., Balco, G., Lavé, J., Delunel, R., Lifton, N., Laurent, V., 2017. The CREp program and the ICE-D production rate calibration database: A fully parameterizable and updated online tool to compute cosmic-ray exposure ages. Quat. Geochronol. 38, 25–49. https://doi.org/10.1016/j.quageo.2016.11.006

Merchel, S., Arnold, M., Aumaître, G., Benedetti, L., Bourlès, D.L., Braucher, R., Alfimov, V., Freeman, S.P.H.T., Steier, P., Wallner, A., 2008. Towards more precise 10Be and 36Cl data from measurements at the 10−14 level: Influence of sample preparation. Nucl. Instrum. Methods Phys. Res. Sect. B Beam Interact. Mater. At. 266, 4921–4926. https://doi.org/10.1016/j.nimb.2008.07.031

Moran, A.P., Ivy-Ochs, S., Schuh, M., Christl, M., Kerschner, H., 2016. Evidence of central Alpine glacier advances during the Younger Dryas–early Holocene transition period. Boreas n/a-n/a. https://doi.org/10.1111/bor.12170

Oerlemans, J., 2005. Extracting a Climate Signal from 169 Glacier Records. Science 308, 675–677. https://doi.org/10.1126/science.1107046

Osmaston, H., 2005. Estimates of glacier equilibrium line altitudes by the Area×Altitude, the

871 Area×Altitude Balance Ratio and the Area×Altitude Balance Index methods and their
872 validation. Quat. Int. 138–139, 22–31. https://doi.org/10.1016/j.quaint.2005.02.004
873 Payot, V., 1884. Oscillations des quatre grands glaciers de la vallée de Chamonix et
874 énumération des ascensionnistes au Mont-Blanc. Sandoz, Genève.
875 Pellitero, R., Rea, B.R., Spagnolo, M., Bakke, J., Hughes, P., Ivy-Ochs, S., Lukas, S.,
876 Ribolini, A., 2015. A GIS tool for automatic calculation of glacier equilibrium-line altitudes.
877 Comput. Geosci. 82, 55–62. https://doi.org/10.1016/j.cageo.2015.05.005
878 Pellitero, R., Rea, B.R., Spagnolo, M., Bakke, J., Ivy-Ochs, S., Frew, C.R., Hughes, P.,
879 Ribolini, A., Lukas, S., Renssen, H., 2016. GlaRe, a GIS tool to reconstruct the 3D surface of
880 palaeoglaciers. Comput. Geosci. 94, 77–85. https://doi.org/10.1016/j.cageo.2016.06.008
881 Rabatel, A., Letréguilly, A., Dedieu, J.-P., Eckert, N., 2013. Changes in glacier equilibrium-
882 line altitude in the western Alps from 1984 to 2010: evaluation by remote sensing and
883 modeling of the morpho-topographic and climate controls. The Cryosphere 7, 1455–1471.
884 https://doi.org/10.5194/tc-7-1455-2013
885 Rabatel, A., Sanchez, O., Vincent, C., Six, D., 2018. Estimation of Glacier Thickness From
886 Surface Mass Balance and Ice Flow Velocities: A Case Study on Argentière Glacier, France.
887 Front. Earth Sci. 6. https://doi.org/10.3389/feart.2018.00112
888 Rea, B.R., 2009. Defining modern day Area-Altitude Balance Ratios (AABRs) and their use
889 in glacier-climate reconstructions. Quat. Sci. Rev. 28, 237–248.
890 https://doi.org/10.1016/j.quascirev.2008.10.011
891 Renssen, H., Goosse, H., Roche, D.M., Seppä, H., 2018. The global hydroclimate response
892 during the Younger Dryas event. Quat. Sci. Rev. 193, 84–97.
893 https://doi.org/10.1016/j.quascirev.2018.05.033
894 Réveillet, M., Vincent, C., Six, D., Rabatel, A., 2017. Which empirical model is best suited to
895 simulate glacier mass balances? J. Glaciol. 63, 39–54. https://doi.org/10.1017/jog.2016.110
896 Scherler, D., Bookhagen, B., Strecker, M.R., 2011. Spatially variable response of Himalayan
897 glaciers to climate change affected by debris cover. Nat. Geosci. 4, 156–159.
898 https://doi.org/10.1038/ngeo1068
899 Schimmelpfennig, I., Schaefer, J.M., Akçar, N., Koffman, T., Ivy-Ochs, S., Schwartz, R.,
900 Finkel, R.C., Zimmerman, S., Schlüchter, C., 2014. A chronology of Holocene and Little Ice
901 Age glacier culminations of the Steingletscher, Central Alps, Switzerland, based on high-
902 sensitivity beryllium-10 moraine dating. Earth Planet. Sci. Lett. 393, 220–230.
903 https://doi.org/10.1016/j.epsl.2014.02.046
904 Schindelwig, I., Akçar, N., Kubik, P.W., Schlüchter, C., 2012. Lateglacial and early Holocene

dynamics of adjacent valley glaciers in the Western Swiss Alps. J. Quat. Sci. 27, 114–124. https://doi.org/10.1002/jqs.1523

Schwander, J., Eicher, U., Ammann, B., 2000. Oxygen isotopes of lake marl at Gerzensee and Leysin (Switzerland), covering the Younger Dryas and two minor oscillations, and their correlation to the GRIP ice core. Palaeogeogr. Palaeoclimatol. Palaeoecol. 159, 203–214. https://doi.org/10.1016/S0031-0182(00)00085-7

Six, D., Vincent, C., 2014. Sensitivity of mass balance and equilibrium-line altitude to climate change in the French Alps. J. Glaciol. 60, 867–878. https://doi.org/10.3189/2014JoG14J014

Smiraglia, C., Azzoni, R.S., D'Agata, C., Maragno, D., Fugazza, D., Diolaiuti, G.A., 2015. The evolution of the Italian glaciers from the previous data base to the New Italian Inventory. Preliminary considerations and results. Geogr. Fis. E Din. Quat. 38, 79–87.

Smiraglia, C., Diolaiuti, G., Casati, D., Kirkbride, M.P., 2010. Recent areal and altinietric variations of Miage Glacier (Monte Bianco massif, Italian Alps) 264, 7.

Solomina, O.N., Bradley, R.S., Jomelli, V., Geirsdottir, A., Kaufman, D.S., Koch, J., McKay, N.P., Masiokas, M., Miller, G., Nesje, A., Nicolussi, K., Owen, L.A., Putnam, A.E., Wanner, H., Wiles, G., Yang, B., 2016. Glacier fluctuations during the past 2000 years. Quat. Sci. Rev. 149, 61–90. https://doi.org/10.1016/j.quascirev.2016.04.008

Vincent, C., Le Meur, E., Six, D., Funk, M., 2005. Solving the paradox of the end of the Little Ice Age in the Alps. Geophys. Res. Lett. 32, L09706. https://doi.org/10.1029/2005GL022552

Vincent, C., Soruco, A., Six, D., Le Meur, E., 2009. Glacier thickening and decay analysis from 50 years of glaciological observations performed on Glacier d'Argentière, Mont Blanc area, France. Ann. Glaciol. 50, 73–79.

Wurth, G., Niggemann, S., Richter, D.K., Mangini, A., 2004. The Younger Dryas and Holocene climate record of a stalagmite from Hölloch Cave(Bavarian Alps, Germany. J. Quat. Sci. 19, 291–298. https://doi.org/10.1002/jqs.837

Young, N.E., Schaefer, J.M., Briner, J.P., Goehring, B.M., 2013. A 10Be production-rate calibration for the Arctic. J. Quat. Sci. 28, 515–526. https://doi.org/10.1002/jqs.2642